TECHNISCHE UNIVERSITÄT WIEN
Vienna University of Technology

DIPLOMARBEIT

Set-up of a steady-state heat-flow method for measuring thermal conductivity from 1.5K to room temperature

Ausgeführt am Institut für Festkörperphysik
der Technischen Universität Wien

unter der Anleitung von
Univ.Prof. Dipl.-Ing. Dr.techn. Ernst Bauer

durch
Joachim Jeitler
3913 Großgöttfritz 80

September 2014 _____

Abstract

Thermal conductivity is a physical property of materials which denotes the capability of transporting heat. According to the laws of thermodynamics, heat flows from parts at higher temperatures to parts at lower temperatures. Left to itself, an isolated system will eventually achieve thermal equilibrium – everything is at the same temperature. The speed of this equalization process is directly related to the thermal conductivity. To actually measure thermal conductivity, temperature differences and a corresponding heat flux have to be present.

For measuring purposes, a dynamic thermal equilibrium is desirable, i.e. by keeping two parts of a sample at given (but different) temperatures, a constant heat flux between these parts will be attained. The system is then said to be in a *steady state*. The magnitude of this heat flux is determined by the 'thermal resistance' of the respective material.

Thermal resistance (or its reciprocal, thermal conductivity) is not only dependent on the actual material in question, but also on various physical parameters like temperature, magnetic field, phase, material structure or sample orientation. Knowledge of thermal conductivity in dependency on different external influences gives an insight into underlying physical principles and material-specific properties and therefore helps develop and choose materials for diverse thermal applications.

Therefore this thesis is aimed at the development of a device for measuring the temperature dependent thermal conductivity of solids. It is focused on low temperatures – i.e. from below the boiling point of liquid helium (which is used as a coolant) up to room temperature.

Kurzfassung

Die physikalische Eigenschaft von Materialien, Wärme transportieren zu können, bezeichnet man als *Thermische Leitfähigkeit*. Gemäß den Gesetzen der Thermodynamik fließt Wärme von selbst immer von Bereichen mit höherer Temperatur zu Bereichen mit niedrigerer Temperatur. Ohne äußeren Einfluss wird ein isoliertes System schließlich ein thermisches Gleichgewicht erreichen – alle Teile haben die selbe Temperatur. Die Geschwindigkeit dieses Normalisierungsprozesses hängt direkt von der thermischen Leitfähigkeit ab. Will man die thermische Leitfähigkeit messen, muss natürlich eine Temperaturdifferenz – und damit verbunden ein Wärmefluss – vorliegen.

Für die Messung ist es von Vorteil, wenn ein dynamisches Gleichgewicht vorliegt – wenn zwei Bereiche einer Probe auf definierten, aber unterschiedlichen, Temperaturen gehalten werden, ergibt sich ein konstanter Wärmestrom zwischen diesen Bereichen. Man bezeichnet ein solches Verhalten als stationären Zustand. Die Größe dieses Wärmestroms ergibt sich aus dem „thermischen Widerstand“ des Probenmaterials.

Der thermische Widerstand (oder auch dessen Kehrwert, die thermische Leitfähigkeit) hängt nicht nur vom Probenmaterial ab, sondern auch von einer Vielzahl an physikalischen Parametern, wie Temperatur, magnetischem Feld, Phase, Materialstruktur und -zusammensetzung oder auch Probenorientierung. Kenntnis der thermischen Leitfähigkeit in Abhängigkeit dieser externen Einflüsse erlaubt einen Einblick in die zugrundeliegenden physikalischen Prinzipien und materialspezifischen Eigenschaften und hilft daher bei der Entwicklung und Auswahl von Materialien für diverse thermische Anwendungen.

Das Ziel dieser Diplomarbeit war es, eine Anlage zur Messung von thermischer Leitfähigkeit in Abhängigkeit von der Probentemperatur zu entwickeln. Im Speziellen lag der Fokus auf tiefen Temperaturen – von unter dem Siedepunkt von flüssigem Helium (das auch als Kühlmittel dient) bis hin zu Raumtemperatur.

Acknowledgement

First of all, I would like to thank my thesis supervisor Ernst Bauer, who has provided me not only with an interesting task, but also with support whenever needed. His door was literally open all the time for any request and his good-natured manner is positively responsible for the good atmosphere within the entire group.

Special mentioning is deserved by Herbert Müller, who was essential in building the software to the measurement system. He was always ready to answer any remaining questions, be they of constructional, procedural or software-related manner and essentially became a second supervisor to me.

Many thanks to my co-workers and colleagues at the Institute of Solid State Physics and its workshop. Various diploma and doctoral students have helped in many ways – some related to the work, some more circumstantially. Representatively I would like to point out Norbert Ackerl, Friedrich Kneidinger and Matthias Ikeda.

To all my friends from university (from within the Fachschaft Physik and without) and from back home: Thank you for all these wonderful years, you have really enriched my life. During all this time we shared a lot of work and fun (and honestly, we managed to make most of the work seem like fun, too). May we never lose contact!

Special thanks for 'dragging me over the finishing line' go to Robert Hollenstein and Jörg Herzinger. You and the entire *Els* gang are the best!

Last, but definitely not least, I would like to express my gratitude to my family, especially my parents, for their never-ending support. Throughout the studies they kept believing in me and helped me get through all troubles. Thank you!

This thesis was financially supported by the FP7 NanoHiTEC research programme.

Contents

1. Theoretical background

Transport Phenomena is a collective term describing exchange and conductance processes of variable physical quantities as a result of external driving forces. Prominent examples are thermal and electrical conductivity, Seebeck, Peltier or Hall effects. The knowledge of these transport processes allows insights into the electronic and phononic structure and properties of diverse materials. As the purpose of this thesis is the set-up of a measuring device for thermal conductivity, special attention on it will be allotted here.

The basic deductions and theoretical considerations in this chapter, unless otherwise noted, mostly follow the reasoning of the fundamental solid state and quantum mechanic works [1–4].

Thermal conductivity denotes the property to transfer heat within a material along a temperature gradient. As known from observation, heat flows from a hot environment to a cold one. The vector $\vec{j}$ of heat flux density points in opposite direction of an occurring temperature gradient $\vec{\nabla}T$:

$$\vec{j} = -\lambda \vec{\nabla} T \tag{1.1}$$

λ is the coefficient of thermal conductivity, a positive, material- and temperature-dependent factor. From the kinetic theory of gases the following expression for thermal conductivity can be derived:

$$\lambda = \frac{1}{3} C v l \tag{1.2}$$

C stands for the specific heat per volume, v for the mean particle velocity and l for the mean free path. For solids, a starting model can be a perfect crystal lattice, acting only as background to the various excitations that contribute to the observable phenomena. These excitations influence the thermodynamic properties and their propagations. In an anology to the kinetic theory of gases, thermal conductivity can be described by an expression similar to equation 1.2. Each excitation can be

accounted for by a corresponding particle and/or wave. Therefore one has to sum over all contributions, using their respective mean velocities, mean free paths and contributions to the specific heat per volume.

$$\lambda = \frac{1}{3} \sum_j C_j v_j l_j \tag{1.3}$$

In solids, the main contributors to thermal conductivity are lattice waves and free electrons, therefore these will be highlighted here.

1.1. Electronic Contribution

Starting with free electrons and treating them as a Fermi gas, equation 1.2 can be used to obtain the thermal conductivity. When putting a free electron into a periodic lattice, its eigenfunction has to change due to the electric potential of the lattice. Translational periodicity in a lattice can be implemented by a translation vector $\vec{T} = \sum_i n_i \vec{a}_i$, with n_i being arbitrary integer numbers and $\vec{a}_i$ the lattice's basis vectors; the lattice parameter will be called a.

A perfect crystal has periodic potential: $U(\vec{r}) = U(\vec{r}+\vec{T})$. To be perfectly periodic, even boundary conditions have to be periodic: when the crystal dimensions are L_i, the potential has to be periodic in L_i ($U(\vec{r}) = U(\vec{r} + L_i \cdot \vec{a}_i)$) as well.

When solving the Schrödinger equation the electron eigenfunctions $\psi_{\vec{k}}$ take the shape of modulated plane waves, the so called Bloch-waves

$$\psi_{\vec{k}}(\vec{r}) = V^{-\frac{1}{2}}\, u_{\vec{k}}(\vec{r})\, \mathrm{e}^{\mathrm{i}\vec{k}\vec{r}}, \tag{1.4}$$

$\vec{k}$ is the wave vector of the electron state, V the crystal volume and $u_{\vec{k}}(\vec{r})$ is a modulating function, it shows the same periodicity as the potential ($u_{\vec{k}}(\vec{r}) = u_{\vec{k}}(\vec{r} + \vec{T})$).

In an ideal crystal the electrons share some properties with free electrons. Whereas the momentum $\vec{p}$ still can be expressed as $\vec{p} = \hbar\vec{k}$, the energy E now becomes some function of $\vec{k}$. Likewise, the electron velocity is not in a simple relationship with the momentum but dependent on $\vec{k}$ ($\vec{v} = \hbar^{-1}\, \partial E/\partial\vec{k}$).

Any periodic lattice has a corresponding periodic reciprocal lattice in $\vec{k}$ space. A reciprocal translation vector $\vec{G}$ can be defined analogously: $\vec{G} = \sum_i m_i \vec{b}_i$. $\vec{b}_i$ are the basis vectors of the reciprocal lattice, m_i arbitrary integers, in case of the reciprocal lattice also called Miller Indices. The reciprocal basis vectors are given by $\vec{b_i} =$

$2\pi \frac{\vec{a}_j \times \vec{a}_k}{V_k}$, V_k is the volume of an elementary cell in the reciprocal lattice ($V_k = \vec{b}_1 \cdot (\vec{b}_2 \times \vec{b}_3)$). As real space and $\vec{k}$ space are dual spaces, their basis vectors are associated by the relation $\vec{a}_i \cdot \vec{b}_j = 2\pi\delta_{ij}$. The dispersion relation $E(\vec{k})$ and the wave function are periodic in $\vec{k}$ space:

$$E(\vec{k}) = E(\vec{k} + \vec{G}) \tag{1.5}$$

$$\psi_{\vec{k}}(\vec{r}) = \psi_{\vec{k}+\vec{G}}(\vec{r}) \tag{1.6}$$

Following from these periodicities is the fact that all information has to be contained in the primitive elementary cell of the reciprocal lattice. This cell is also called the first Brillouin zone. For a periodic crystal, $\vec{k}$ can only have discrete values, linear integer combinations of $2\pi/L_i$. An element of $\vec{k}$ space therefore contains $\frac{V}{(2\pi)^3}\,\mathrm{d}^3\vec{k}$ values for $\vec{k}$. Each state can be occupied only by a single electron, according to the Pauli exclusion principle; if the electrons' spins do not have to be considered, every $\vec{k}$ value can be associated with two electrons.

Real crystal systems are not perfectly periodic, as lattice defects or thermal lattice vibrations disturb the electron wave functions $\psi_{\vec{k}}(\vec{r})$. Therefore these are not stationary but rather a collection of quasi-stationary states. The large number of states and multitude of scattering processes prohibit direct calculation, but in a thermodynamic equilibrium they can be statistically derived. The average occupation number f_0 of a state $\vec{k}$ is given by a Fermi-Dirac distribution

$$f_0(\vec{k}) = \left(\mathrm{e}^{\frac{E(\vec{k})-\mu}{k_B T}} + 1 \right)^{-1}. \tag{1.7}$$

k_B is the Boltzmann constant ($k_B \approx 1,38 \cdot 10^{-23}\,\mathrm{JK}^{-1}$). μ is the chemical potential, which is defined by the number of electron states in the energy interval $\mathrm{d}E$, $n(E)\mathrm{d}E$:

$$\int n(E) f_0(E, \mu, T)\mathrm{d}E = N_e, \tag{1.8}$$

with N_e being the total number of electrons.

The deduction of thermal conductivity (or other transport phenomena) is performed by calculating the distribution function $f(\vec{r}, \vec{k}, t)$ in dependence on external fields. Upon the influence of external fields and scattering processes the initially homogeneous equilibrium distribution assumes a spatial and time dependency

($f_0 \to f(\vec{r}, \vec{k}, t)$). After a time interval dt, f evolves to

$$f(\vec{k} + \dot{\vec{k}}\mathrm{d}t, \vec{r} + \dot{\vec{r}}\mathrm{d}t, t + \mathrm{d}t) = f(\vec{k}, \vec{r}, t) + \left(\frac{\partial f}{\partial t}\right)_{coll} \mathrm{d}t, \tag{1.9}$$

the index *coll* denotes the collision term. By Taylor expansion and equating coefficients, this equation leads to the Boltzmann equation:

$$\left(\frac{\partial}{\partial t} + \dot{\vec{k}} \cdot \vec{\nabla}_{\vec{k}} + \dot{\vec{r}} \cdot \vec{\nabla}_{\vec{r}}\right) f\left(\vec{k}, \vec{r}, t\right) = \left(\frac{\partial f}{\partial t}\right)_{coll} \tag{1.10}$$

External electrical fields and temperature gradients shall be considered in detail: An external electrical field $\vec{E}$ interacts with electrons by accelerating them against the field vector. Their momentum changes by $\hbar\dot{\vec{k}} = e\vec{E}$, with e the electric charge of an electron. A temperature gradient causes the electron distribution to be dependent on position $\vec{r}$, the different temperatures leading to different electron velocities as the electrons are moving through the solid. Therefore the occupation number is changed by external influences as follows:

$$\left.\frac{\mathrm{d}f}{\mathrm{d}t}\right|_{\vec{E}} = \frac{e\vec{E}}{\hbar} \cdot \vec{\nabla}_{\vec{k}} f_0 \tag{1.11}$$

$$\left.\frac{\mathrm{d}f}{\mathrm{d}t}\right|_{\vec{\nabla}T} = -\dot{\vec{r}} \cdot \vec{\nabla}_{\vec{r}} f_0 \tag{1.12}$$

Countering this tendency to disturb the equilibrium distribution are scattering processes caused by crystal defects and lattice vibrations. They can be described by a relaxation time ansatz with a characteristic time τ

$$\left.\frac{\mathrm{d}f}{\mathrm{d}t}\right|_{ext.} = -\frac{f(\vec{k}) - f_0(\vec{k})}{\tau(\vec{k})} = -\frac{g(\vec{k})}{\tau(\vec{k})}\,, \tag{1.13}$$

where $g(\vec{k})$ is the deviation between the disturbed distribution and the equilibrium. Under the driving force of stationary external influences and relaxation processes, a steady state will eventually be reached. Stationarity implies that the first term in the Boltzmann equation 1.10 ($\frac{\partial f}{\partial t}$) vanishes. The deviation $g(\vec{k})$ can therefore be

expressed as

$$g(\vec{k}) = -\tau(\vec{k})\frac{\mathrm{d}f_0}{\mathrm{d}E}\,\dot{\vec{r}}\cdot\left(e\vec{E} - k_B\left(\frac{E-\mu}{k_BT} + \frac{1}{k_B}\frac{\mathrm{d}\mu}{\mathrm{d}T}\right)\vec{\nabla}T\right). \tag{1.14}$$

By using this expression electric and thermal current densities ($\vec{j}_{el}$ and $\vec{j}_Q$, respectively) can be further defined. As these currents vanish in equilibrium states, they are linear in $\vec{g}$.

$$\vec{j}_{el} = \frac{2e}{(2\pi)^3}\int \dot{\vec{r}}(\vec{k})\,g(\vec{k})\,\mathrm{d}^3\vec{k} \tag{1.15}$$

$$\vec{j}_Q = \frac{2}{(2\pi)^3}\int \dot{\vec{r}}\Big(E(\vec{k}) - \mu\Big)\,g(\vec{k})\,\mathrm{d}^3\vec{k} \tag{1.16}$$

As

$$\lambda = -\frac{\vec{j}_Q}{\vec{\nabla}T} \tag{1.17}$$

is only valid when $\vec{j}_{el} = 0$, the electrical current and conductivity has to be considered as well. By converting the integration over $\vec{k}$ space to an integration over electron energy and surfaces of constant E in $\vec{k}$ space ($\mathrm{d}^3\vec{k} = \mathrm{d}E\,\mathrm{d}A/(\mathrm{d}E/\mathrm{d}k)_n$), the correlation with $g(\vec{k})$ being a function of $\mathrm{d}f_0/\mathrm{d}E$ can be harnessed. $(\mathrm{d}E/\mathrm{d}k)_n$ is the derivative perpendicular to levels of equal energy and $\mathrm{d}A$ is a surface element in $\vec{k}$ space.

In case of isothermality, the electric current density can be defined by a conductivity tensor σ_{ij}.

$$\vec{j}_{el} = \sigma_{ij}\cdot\vec{E}, \qquad \sigma_{ij} = -\int \frac{\mathrm{d}f_0}{\mathrm{d}E}\;\sigma_{ij}(E)\;\mathrm{d}E \tag{1.18}$$

$$\sigma_{ij}(E) = \frac{2e^2}{(2\pi)^3}\int_E \mathrm{d}A\;\frac{\tau(\vec{k})\,\dot{r}_i\dot{r}_j}{\left|\vec{\nabla}_{\vec{k}}E\right|} \tag{1.19}$$

If the relaxation time τ is a unique function of $\vec{k}$, both $\vec{j}_{el}$ and $\vec{j}_Q$ can be written in dependence on $\sigma(E)$:

$$\vec{j}_{el} = \left(\vec{E} - \frac{1}{e}\frac{\mathrm{d}\mu}{\mathrm{d}T}\vec{\nabla}T\right)M_0 - \frac{k_B}{e}\;\vec{\nabla}TM_1 \tag{1.20}$$

$$\vec{j}_Q = \frac{k_BT}{e}\left(\vec{E} - \frac{1}{e}\frac{\mathrm{d}\mu}{\mathrm{d}T}\vec{\nabla}T\right)M_1 - \frac{k_B^2T}{e^2}\;\vec{\nabla}TM_2, \tag{1.21}$$

with

$$M_0 = -\int \sigma(\varepsilon)\,\frac{\mathrm{d}f_0}{\mathrm{d}\varepsilon}\,\mathrm{d}\varepsilon \tag{1.22}$$

$$M_1 = -\int \sigma(\varepsilon)\varepsilon\,\frac{\mathrm{d}f_0}{\mathrm{d}\varepsilon}\,\mathrm{d}\varepsilon \tag{1.23}$$

$$M_2 = -\int \sigma(\varepsilon)\varepsilon^2\,\frac{\mathrm{d}f_0}{\mathrm{d}\varepsilon}\,\mathrm{d}\varepsilon \tag{1.24}$$

$$\varepsilon = \frac{E-\mu}{k_B T} \tag{1.25}$$

When no electrical current is present, equation 1.20 equals zero and can be inserted in equation 1.21. Division by $-\vec{\nabla}T$ as per equation 1.17 yields the electronic thermal conductivity

$$\lambda_e = \frac{k_B^2\,T}{e^2}\left(M_2 - \frac{{M_1}^2}{M_0}\right) \tag{1.26}$$

1.2. Lattice Contribution

In addition to the electrons taking part in thermal conductivity, there is also a contribution due to the lattice and its vibrations. In insulators these are the main thermal transportation processes, due to the lack of conduction electrons. The lattice atoms vibrate around their equilibrium positions, for small displacements the resulting oscillations can be described as harmonic oscillators. But as each atom does not have a fixed equilibrium position in the lattice (because it is influenced by surrounding atoms and their relative positions), the resulting oscillations are not independent of each other but form a system of coupled equations. This system of coupled equations for each individual atom can be translated into a superposition of propagating lattice waves. Hence the displacement $\vec{u}(\vec{r})$ can be written in terms of a wave vector $\vec{q}$:

$$\vec{u}(\vec{r}) = \frac{1}{\sqrt{N_l}}\sum_{\vec{q},j}\vec{e}_j b_j(\vec{q})\,\mathrm{e}^{\mathrm{i}(\vec{q}\cdot\vec{r}+\omega t)} \tag{1.27}$$

N_l is the total number of lattice points, j the polarisation index, $\vec{e}_j$ is the unit vector of said polarisation, b_j is the wave's amplitude, ω its angular frequency. As the same boundary conditions apply for the lattice waves as for the electron waves, restrictions similar to the number of admissible $\vec{k}$ are in effect: in an element $\mathrm{d}\vec{q}$ in $\vec{q}$ space there are $\frac{V}{(2\pi)^3}\,\mathrm{d}\vec{q}$ values for $\vec{q}$. Once again, all physical properties can be obtained by observing the first Brillouin zone.

In an elastic continuum there are three different modes of oscillation: One with

a direction of polarisation parallel to $\vec{q}$ (longitudinal wave) and two with polarisations perpendicular to $\vec{q}$ (transversal waves), the longitudinal wave posesses the highest frequency. In a discrete lattice, there is no such simple association between $\vec{q}$ and polarisation (the polarisations are still mutually perpendicular to each other), although there is still the tendency to call the wave with highest frequency longitudinal. For simplicity's sake, explicit references to polarisation will be omitted from now on, the polarisation can be thought to be included in the wave vector $\vec{q}$.

In a lattice with more than one atom in its irreducible unit cell, in addition to the three already mentioned (*acoustic*) modes, there are $3r - 3$ *optical* modes, with r the number of (not necessarily different) atoms in the lattice's irreducible unit cell.

For lattice waves, phase velocity $\vec{v}_p$ and group velocity $\vec{v}_g$ differ in general:

$$\vec{v}_p = \frac{\omega}{\vec{q}} \tag{1.28}$$

$$\vec{v}_g = \frac{\partial\omega}{\partial\vec{q}} \tag{1.29}$$

By summing over all wave vectors $\vec{q}$ and polarisations j in equation 1.27 all normal modes of the crystal are described. Each normal mode possesses an energy of

$$E(\vec{q}) = m\omega^2 b^*(\vec{q})\, b(\vec{q}), \tag{1.30}$$

m is the elementary mass (i.e. the mass of each atom or the unit cell), b^* is the complex conjugate of the amplitude b. The oscillation energy of the whole crystal is the sum over the energy of all normal modes.

For small displacements the restoring force can be assumed to follow Hooke's law and therefore the resulting oscillations to be harmonic oscillations. In quantum theory the energy of a harmonic oscillator is shown to exist only in discrete levels

$$E(\vec{q}) = \hbar\omega\left(n + \frac{1}{2}\right), \tag{1.31}$$

where n is an integer ≥ 0. Above a zero-point energy of $\hbar\omega/2$ there are discrete steps in energy, these quanta can be described as quasi-particles called phonons.

Quantum-mechanical ladder operators for transitions between different states can be specified as well. By defining

$$a(\vec{q}) = b(\vec{q})\, \mathrm{e}^{\mathrm{i}\omega t} \tag{1.32}$$

the Hamiltonian (the operator corresponding to the total energy) can be written as

$$H = \sum_{\vec{q}} H(\vec{q}) = \sum_{\vec{q}} \frac{m\omega^2}{2} \left(a^*(\vec{q}) a(\vec{q}) + a(\vec{q}) a^*(\vec{q}) \right). \tag{1.33}$$

Quantum-mechanically the continuous $a(\vec{q})$ have to be replaced by matrices. By cleverly choosing these matrices, a and $a^\dagger$ (the matrix gets transposed as well as conjugated) can be interpreted as annihilation and creation operators, respectively. The creation operator $a^\dagger$ increases the number of phonons in the mode in question by one, likewise the annihilation operator a decreases it by one; their product yields the occupation number operator: $a^\dagger a = N$.

These theoretical considerations are fully valid only for perfect lattices. Only there the energy of each normal mode $E(\vec{q})$ is a constant of motion, and the number and distributions of phonons $N(\vec{q})$ are conserved. Real crystals – apart from naturally having non-periodic boundary conditions – also have all sorts of lattice defects and impurities. Therefore, the lattice modes can no longer be considered as normal modes and an interchange of energy between lattice waves becomes possible. A statistical equilibrium will be reached eventually; as phonons have a spin of 0 and therefore are bosons, the distribution function will resemble Bose-Einstein statistics:

$$N_0(\vec{q}) = \left(\mathrm{e}^{\frac{\hbar\omega}{k_B T}} - 1 \right)^{-1}. \tag{1.34}$$

A temperature gradient will perturb this equilibrium distribution. An ansatz similar to the electronic case (1.9) can be used:

$$\left. \frac{\mathrm{d}N}{\mathrm{d}t} \right|_{\vec{\nabla} T} = - \vec{v}_g \cdot \vec{\nabla} N_0 \tag{1.35}$$

Once again it is helpful to define the deviation from equilibrium ($n(\vec{q})$) and propose that the return to equilibrium by scattering and interaction processes is coupled to a characteristic relaxation time τ.

$$\left. \frac{\mathrm{d}N}{\mathrm{d}t} \right|_{int.} = - \frac{N(\vec{q}) - N_0(\vec{q})}{\tau(\vec{q})} = - \frac{n(\vec{q})}{\tau(\vec{q})} \tag{1.36}$$

In case of a stationary temperature gradient a steady state will be reached and as

$\frac{\mathrm{d}N}{\mathrm{d}T}$ equals zero, the deviation can be expressed as

$$n(\vec{q}) = -\tau(\vec{q})\,(\vec{v}_g \cdot \vec{\nabla} N) = -\tau(\vec{q})\,(\vec{v}_g \cdot \vec{\nabla} T)\,\frac{\mathrm{d}N_0}{\mathrm{d}T}. \tag{1.37}$$

The heat current $\vec{j}_Q$ depends on the phonon distribution $N(\vec{q})$, but as in an equilibrium there is no effective heat current, the deviation can be used instead:

$$\vec{j}_Q = \sum_{\vec{q}} \vec{v}_g \hbar\omega\, n(\vec{q}) \tag{1.38}$$

Using equation 1.17, an expression for the lattice contribution to thermal conductivity can be derived:

$$\lambda_l = \sum_{\vec{q}} \left(\vec{v}_g \cdot \vec{e}_{j_Q}\right)^2 \tau(\vec{q})\, c(\vec{q}), \tag{1.39}$$

with $\vec{e}_{j_Q}$ a unit vector parallel to the heat flow and $c(\vec{q})$ the contribution to specific heat by a single mode $\vec{q}$, $c(\vec{q}) = \hbar\omega \frac{\mathrm{d}N_0}{\mathrm{d}T}$.

1.3. Interaction and Scattering Processes

In addition to these static considerations, interactions have to be borne in mind. These interactions can change the state the system is in. Considering two sets of states, i and j, the associated energies are denoted E_i, E_j (ΔE is the difference $E_i - E_j$), the probabilities to find a system in such a state are W_i and W_j. A perturbation Hamiltonian H'_{ij} is associated with a change between states i and j. The effective change to the probability to find a system in state i is

$$W_i(t) - W_i(0) = 2\sum_j (H'_{ij})^2\, \frac{1 - \cos(\frac{\Delta E\, t}{\hbar})}{\Delta E^2}. \tag{1.40}$$

The fraction describes a resonance factor that favours processes in the vicinity of $\Delta E = 0$. The finding of this probability boils down to get estimations for the H'_{ij} for all possible interacting states j.

1.3.1. Phonon Scattering

Since phonon scattering processes by deviations from the perfect lattice or between phonons themselves limit their mean free path, it will be necessary to look at these interaction. In section 1.2 the Hamiltonian for an unperturbed system was given in

equation 1.33. Expanding the equation to accommodate two phonons ($\vec{q}$ and $\vec{q}'$), the unperturbed Hamiltonian of a perfect solid reads

$$H_0 = \frac{1}{N_l} \sum_{\vec{r}} \sum_{\vec{q},\vec{q}'} m\omega\omega' \mathrm{e}^{\mathrm{i}(\vec{q}-\vec{q}')\cdot\vec{r}}\ \vec{a}^{\dagger}(\vec{q}')\, a(\vec{q})\,. \tag{1.41}$$

When summing over all lattice points $\vec{r}$ and all pairs of waves ($\vec{q}$, $\vec{q}'$) only terms with $\vec{q} = \vec{q}'$ do not cancel each other out and the Hamiltonian simplifies to

$$H_0 = \sum_{\vec{q}} m\omega^2 a^{\dagger}(\vec{q})\, a(\vec{q}) \tag{1.42}$$

In this unperturbed Hamiltonian, each contribution to the sum describes the creation and ensuing annihilation of a phonon $\vec{q}$, therefore the system stays unchanged. An actual perturbation to the system leads to a Hamiltonian that changes the system:

$$H' = \sum_{\vec{q},\vec{q}'} c_2(\vec{q},\vec{q}')\, a^{\dagger}(\vec{q}')\, a(\vec{q}) \tag{1.43}$$

$$H' = \sum_{\vec{q},\vec{q}',\vec{q}''} c_3(\vec{q},\vec{q}',\vec{q}'')\, a^{\dagger}(\vec{q}'')\, a(\vec{q}')\, a(\vec{q}) \tag{1.44}$$

Equation 1.43 describes the creation of a phonon $\vec{q}'$ and the destruction of a phonon $\vec{q}$, i.e., the scattering of a phonon from a mode $\vec{q}$ into $\vec{q}'$. Equation 1.44 likewise refers to a three-phonon-process where two phonons $\vec{q}$ and $\vec{q}'$ are combined to a phonon $\vec{q}''$. c_2 and c_3 are perturbation coefficients for two- or three-phonon interactions. In a continuum approximation for ω the relation $\omega = vq$ holds.

For the scattering of phonons v is considered to be perturbed by δv at the site r_0 of scattering. The perturbation coefficient c_2 then reads

$$c_2 = \frac{2mv}{N_l} qq' \sum_{\vec{r}} \delta v(\vec{r})\, \mathrm{e}^{\mathrm{i}(\vec{q}-\vec{q}')\vec{r}} \tag{1.45}$$

When squaring H' the exponential term disappears if only a single site $\vec{r}_0$ is perturbed, therefore the scattering is independent of the site.

Scattering sources can also be defined by strain fields. Strains change the local characteristics in a solid, the velocity of (sound) waves near such a strain $\vec{\epsilon}$ changes to

$$\vec{v} = \vec{v}_0\,(\mathbb{1} - \gamma\vec{\epsilon})\,, \quad \delta\vec{v}(\vec{r}) = -\gamma\vec{\epsilon}(\vec{r}). \tag{1.46}$$

γ is the Grüneisen parameter when the directions of the strain and polarisation lead

to dilatation, for shear it is assumed to be similar.

The nature of the strain field determines the scattering process: for static strain fields (stemming from imperfection in the lattice) two-phonon-interactions (see equation 1.43) can be used, for dynamic strain fields (represented by a lattice wave) three-phonon-interactions (see equation 1.44) are applicable.

As demonstrated in [5–7], a static strain's perturbation coefficient can be written as

$$c_2(\vec{q},\vec{q}') = \frac{2m}{\sqrt{3}N_l a^3}\omega\omega' E(\vec{q}'-\vec{q}), \tag{1.47}$$

with $E(\vec{q})$ being the Fourier inversion of the strain field:

$$E(\vec{q}) = \int \vec{\epsilon}(\vec{x})\, \mathrm{e}^{-\mathrm{i}\vec{q}\cdot\vec{r})}\mathrm{d}\vec{r} \tag{1.48}$$

In a similar vein, the coefficient for a dynamic strain (involving three phonons) can be determined:

$$c_3(\vec{q},\vec{q}',\vec{q}'') = -\mathrm{i}\sqrt{\frac{1}{3N_l^3}}\,\frac{2m\gamma}{v}\omega\omega'\omega''\left(\sum_{\vec{r}}\,\mathrm{e}^{\mathrm{i}(\vec{q}+\vec{q}'-\vec{q}'')\cdot\vec{r}}\right) \tag{1.49}$$

Due to the summation over all lattice points $\vec{r}$ the bracket term vanishes, unless either

$$\vec{q}+\vec{q}'-\vec{q}''=0 \qquad \text{or} \tag{1.50a}$$

$$\vec{q}+\vec{q}'-\vec{q}''=\vec{G} \tag{1.50b}$$

is satisfied, in which case the bracket term simple becomes N_l. For the purpose of this derivation, an interaction $\vec{q}+\vec{q}' \rightarrow \vec{q}''$ is reviewed; for different processes changes of sign have to be heeded, but the essence of the considerations stays the same.

While the adherence to the resonance factor (cf. equation 1.40) – only processes in which $\omega+\omega'=\omega''$ prevails – accounts for conservation of energy, equations 1.50a and 1.50b refer to the conservation of momentum by defining a pseudo-momentum $\hbar\vec{q}$. Processes which follow equation 1.50a are called *Normal* or N-processes.

If the resulting phonon's wave vector points out of the first Brillouin zone, it can be thought of getting scattered back into the the zone by subtracting a reciprocal lattice vector $\vec{G}$. The corresponding momentum $\hbar\vec{G}$ is transferred to the lattice. These processes are called *Umklapp* or U-process, stemming from the German word 'umklappen', which means 'to turn over, to fall over', a phrase used by Rudolf Peierls

when he discovered this theory [8].

N-processes do not contribute to thermal resistivity – as the total phonon momentum is conserved, a non-vanishing phonon momentum will stay unchanged. Therefore a thermal equilibrium cannot be reached; the thermal conductivity of a (perfect, infinite, boundary-less) crystal without Umklapp-processes would be infinite.

1.3.2. Electron Scattering

Electron scattering at lattice defects can be treated in a manner similarly to the phononic case. While a perfectly periodic potential does not scatter electrons (but shape the electron eigenfunction into Bloch-waves, see section 1.1), a disturbed potential $U'(\vec{r})$ leads to a perturbation Hamiltonian for two states $\vec{k}$ and $\vec{k}'$

$$H'_{\vec{k}',\vec{k}} = \int \psi^*_{\vec{k}'}\, U'(\vec{r})\, \psi_{\vec{k}}\, \mathrm{d}\vec{r}. \tag{1.51}$$

In accordance to equation 1.40 the rate of change of the occupation number $f(\vec{k})$ reads

$$t\frac{\mathrm{d}f}{\mathrm{d}t} = 2\sum_{\vec{k}'} \big(\,(1-f)\,f' - f\,(1-f')\,\big)\,\left|H_{\vec{k}',\vec{k}'}\right|^2\,\frac{1-\cos(\frac{\Delta E t}{\hbar})}{\Delta E^2}, \tag{1.52}$$

with $\Delta E = E(\vec{k}') - E(\vec{k})$ in this case. As electrons are fermions, the Pauli exclusion principle has to be considered. Therefore the expressions in the bracket refer to the probabilities of the electron being in state $\vec{k}'$ and not in state $\vec{k}$ initially ($(1-f)f'$) and in state $\vec{k}$ and not in state $\vec{k}'$ finally ($f(1-f')$).

Electron scattering induces not only thermal resistance but at the same time also electrical resistance which is more accessible to measurements. Exact calculations are complicated to carry through as neither the electron wave function $\psi_{\vec{k}}$ nor the perturbation potential $U'(\vec{r})$ are usually known. $U'(\vec{r})$ also gets shielded by the charge redistribution due to the lattice defects. Since this electron scattering usually is elastic ($E(\vec{k}') = E(\vec{k})$), conductivity values are not changed (see section 1.1).

1.3.3. Electron-Phonon Interactions

Electrons can get scattered by passing lattice waves as well, but in this case inelasticities occur, phonons are emitted or absorbed. Similarly to equation 1.27 where the displacement of atoms in a lattice were described, $\xi(\vec{r})$, the spatial derivative of

displacement due to lattice waves can be defined as follows:

$$\xi(\vec{r}) = \frac{1}{\sqrt{N_l}} \sum_{\vec{q},j} (\vec{e}_j \cdot \vec{q})\ \mathrm{e}^{\mathrm{i}\vec{q}\cdot\vec{r}} a_j(\vec{q}) + c.c. \tag{1.53}$$

c.c. denotes the complex conjugate of the entire term, $\vec{e}_j$ is the displacement's unit vector for polarisation j, the term $(\vec{e}_j \cdot \vec{q})$ is applicable for dilatation, for shear it has to be replaced by $(\vec{e}_j \times \vec{q})$. Emitted or absorbed phonons are handled by the annihilation operator a (or creation operator $a^\dagger$, respectively). The perturbation Hamiltonian for these processes is

$$H'_{\vec{k}',\vec{k}} = \frac{1}{\sqrt{N_l}} \sum_{\vec{q},j} \int \mathrm{d}\vec{R}\ (\vec{e}_j \cdot \vec{q})\, C a_j(\vec{q})\ \psi^*_{\vec{k}'}\, \mathrm{e}^{\mathrm{i}\vec{q}\cdot\vec{r}} \psi_{\vec{k}} \quad , \tag{1.54}$$

the integration is performed over all unit cells $\vec{r}$ and all points $\vec{x}$ within the unit cells ($\vec{R} = \vec{r} + \vec{x}$). C is an interaction parameter with the dimension of energy, that depends on the polarisation of the phonons involved.

Each summand in the Hamiltonian refers to an interaction process where an electron is scattered through absorption of a phonon ($\vec{k} + \vec{q} \to \vec{k}'$), or – when considering the conjugate process – through emission of a phonon ($\vec{k} \to \vec{k}' + \vec{q}$).

The integration over $\mathrm{d}\vec{R}$ can be split up into a sum over $\vec{r}$ and an integration over $\vec{x}$. For $\psi_{\vec{k}}$ the Bloch-wave ansatz (see equation 1.4) can be used. The Hamiltonian will then transform to

$$H_{\vec{k}',\vec{k}} = \frac{1}{V\sqrt{N_l}} \sum_{\vec{q},j} C a_j\ (\vec{e}_j \cdot \vec{q}) \left(\left(\sum_{\vec{r}} \mathrm{e}^{\mathrm{i}\vec{r}(\vec{k}+\vec{q}-\vec{k}')} \right) \left(\int \mathrm{d}\vec{x}\, u^*_{\vec{k}'}(\vec{x})\ \mathrm{e}^{\mathrm{i}\vec{x}(\vec{k}-\vec{k}')}\ u_{\vec{k}}\,(\vec{x}) \right) \right) \tag{1.55}$$

The second bracket (with the integration over the unit cell) can be merged into the interaction parameter C. When summing over all lattice sites, the first bracket disappears unless the exponent fulfils either

$$\vec{k} + \vec{q} - \vec{k}' = 0\ , \qquad \text{or} \tag{1.56a}$$

$$\vec{k} + \vec{q} - \vec{k}' = \vec{G}\ . \tag{1.56b}$$

Just as is the case with three-phonon-interactions, equation 1.56a refers to Normal (N) processes, equation 1.56b refers to Umklapp processes, where the wave vector is changed by an inverse lattice vector $\vec{G}$. Looking into the energies involved, the net

energy difference ΔE is

$$\Delta E = E(\vec{k}') - E(\vec{k}) - \hbar\omega \ . \tag{1.57}$$

Once again, the resonance factor $\frac{1-\cos(\Delta E\, t/\hbar)}{\Delta E^2}$ favours processes that adhere to energy conservation.

1.4. Measuring Principle

For measuring thermal conductivity several basic assumptions have to be made. First of all the correlation between heat flux and a temperature gradient can be utilized. As discovered by J. Fourier in 1822 [9], the heat flux is proportional to the temperature gradient responsible for the flux. Therefore, when measuring thermal conductivity (the proportionality coefficient), a temperature gradient has to be applied to the sample. The measuring principle requires that a steady state has been attained. Ideally, all time dependencies vanish before measuring starts and the system is in dynamic equilibrium.

A schematic of the measuring principle can be seen in Figure 1.1.

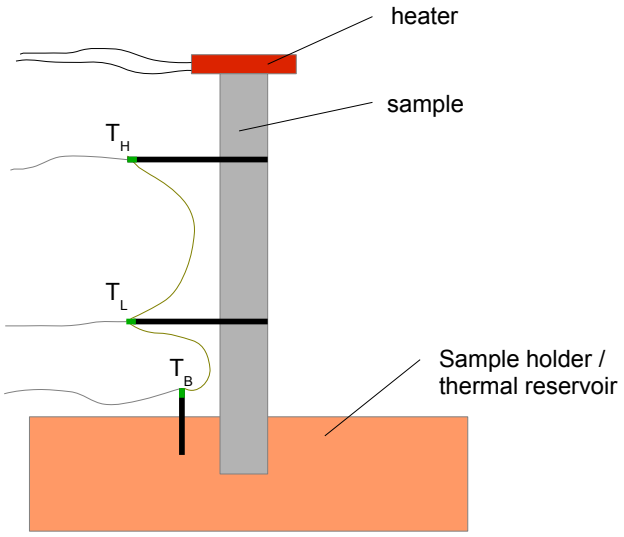

Figure 1.1.: Measuring principle

The sample in question is positioned between an (electric) heater and a thermal reservoir, therefore a temperature gradient is applied to the sample. It has to have a homogeneous cross-section and composition to maintain a constant heat flux density. It will further be assumed that all the heat emitted by the heater flows

through the length of the sample and does not dissipate or radiate away along other paths. Eventually a dynamic thermal equilibrium will be reached and the thermal conductivity can be derived.

The heating power $P = U \cdot I$ of the electrical heater corresponds to the time derivative of the heat being inserted into the system ($\dot{Q}$) and equals the heat flux through the sample cross-section A ($\dot{Q} = \left|\vec{j}_Q\right| \cdot A$).

By measuring the temperature difference between two distinct points along the sample (designated T_H and T_L for high and low temperature, respectively, in figure 1.1) the temperature gradient can be simplified by the temperature difference and the spatial distance l between the points (still assuming a homogeneous gradient warranted by the sample having a constant cross-section).

$$\nabla T \approx \frac{T_H - T_L}{l} = \frac{\Delta T}{l} \tag{1.58}$$

The coefficient of thermal conductivity can therefore be obtained by measuring all constituents of the determining equation

$$\lambda = \frac{\dot{Q}}{\Delta T} \frac{l}{A} \ . \tag{1.59}$$

As thermal conductivity is generally temperature dependent, each measurement also has to specify the temperature of the sample as well. Unfortunately, because of the temperature gradient essential for the measurement, only a mean sample temperature can be stated – and thermal conductivity therefore is not completely homogeneous throughout the sample. A reasonable approximation of the sample temperature (without additional temperature sensors on the sample which would impede the measurement) can be assumed by measuring the temperature of the thermal reservoir and adding the temperature difference between reservoir and lower pick-up (T_B and T_L, see figure 1.1) and half the difference between lower and higher pick-up (T_L and T_H).

As mentioned, thermal conductivity is temperature dependent, and this correlation is of interest. The focus of this diploma thesis lies in the domain below room temperature, hence cooling has to be provided. By both cooling the device by submerging it in liquid gas (inside of a protective and isolating vacuum chamber) and heating the thermal reservoir, any desired temperatures can be set.

2. Experimental Set-up

The following section provides insight into the main part of the diploma thesis, the construction and operation of a device for measuring thermal conductivity at low temperatures.

An overview over the experiment is followed by a more detailed description of the individual components – the scratch-built sample holder and its constituents, the laboratory equipment used, as well as the software used. It is rounded up by a description and an explanation of the actual measurement process.

2.1. Overview

Figure 2.1 shows the schematics of the experimental set-up. It depicts the cryostat with the sample holder inserted, and the arrangement of the various measurement devices, all of which are described in greater detail later in this chapter.

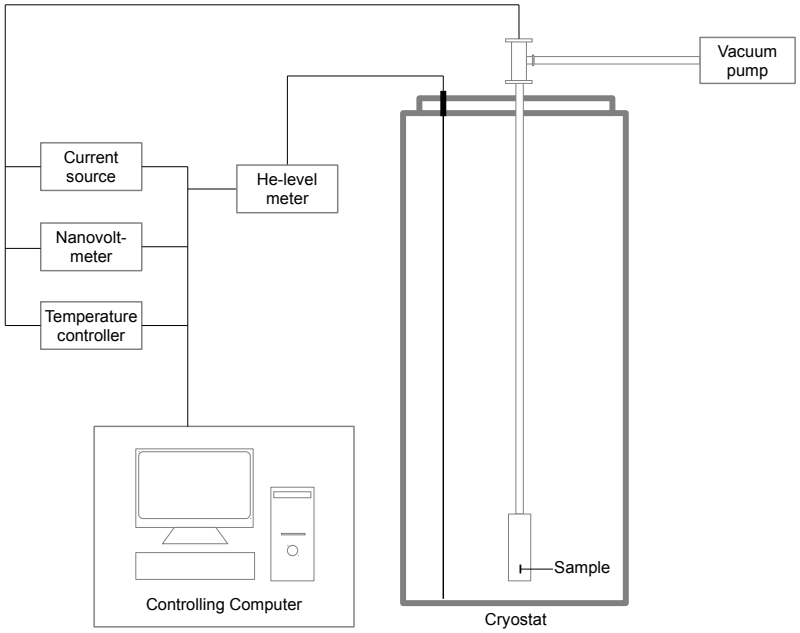

Figure 2.1.: Experimental set-up

To illustrate the drawing, figure 2.2 shows photographs of the actual set-up in the laboratory. In figure 2.2a the sample holder is inserted into a cryostat and connected to the measurement devices visible in the background. The instruments associated with this experiment can be seen in the lower part: at the bottom is the LakeShore Model 336 main temperature controller, on its top are the Keithley 2401 current source (on the left) and the LakeShore Model 335 temperature controller for regulating the helium flow in the continuous-flow cryostat (on the right). Above the current source is the Keithley 2182A nanovoltmeter. On the very top of the rack holding the instruments sits the display of the helium level meter built into the cryostat.

In the background next to the rack, the measurement computer can be (partly) seen. The corresponding monitor and desk workplace are hidden by the cryostat. When conducting an actual measurement, vacuum pumps have to be connected to the sample holder. In 2.2a they are missing, but the flange where the vacuum hose would be connected is clearly visible.

In figure 2.2b the sample holder can be seen in its entire length and next to the continuous-flow cryostat for liquid helium. The cryostat intended for use with liquid nitrogen is directly next to it, on the left-hand side.

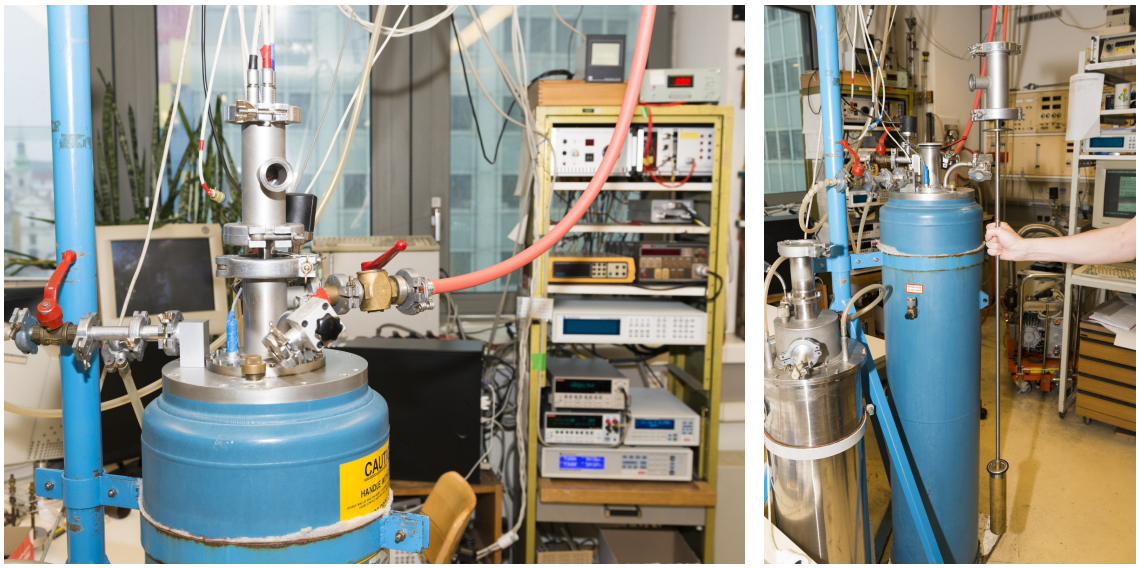

(a) Set-up overview in laboratory (b) Cryostat, sample holder

Figure 2.2.: Measurement Set-up

2.2. Sample Holder

As the sample holder is an integral part of the measurement apparatus, a major part of this diploma work lies in the design and operation of the sample holder. It is designed to operate inside a cryostat to expose the samples to well-defined cryogenic temperatures and connect it to the various measurement devices.

2.2.1. Layout

The sample holder manages samples with a cross-section up to 3 mm by 4 mm and a length of up to about 30 mm. The sample is held in place by a screw-driven chuck. This chuck is made of copper (as is the rest of the sample holder head) due to its very good thermal conductivity throughout the whole temperature range. Enclosing the sample space is a thread-mounted radiation shield to minimize errors due to interfering thermal radiation between sample and environment. To ensure minimal external interaction both the head and the radiation shield have to be kept as close as possible to the same temperature as the sample, therefore both are outfitted with heating elements. For monitoring the temperatures both the head and the radiation shield are outfitted with temperature sensors. The head is linked to the thermal anchor via threaded rods. The anchor acts as a heat sink for all wires and supplies a firm connection to the transition pipe that ends in the sample holder's top which holds the connector plugs to the measurement devices and the flange to the vacuum pump. Surrounding the measurement array is a vacuum cup which separates the measurement device from the cooling agent.

Figure 2.3 shows the sample holder's centrepiece alongside the radiation shield and the vacuum cup. The centrepiece consists of the head on the right-hand side; it is connected via threaded rods to the thermal anchor. The anchor part works as a heat sink for the wires coming down from the sample holder's top (which is at room temperature). The wires are held in place by bands of PTFE[1] , also acting as a protective layer, but obscuring them from view.

The thermal anchor is screwed to the vacuum cup's top plate, which in turn is welded to the stainless steel connecting pipe leading up to the sample holder's top. The brass vacuum cup itself is seen in the top part of figure 2.3. On the bottom the radiation shield with its characteristic red silicon heater mat is pictured. The shield's temperature sensors themselves are hidden from view, but their connecting wires leading to the contact pins are visible.

[1] Polytetrafluoroethylene, also known as Teflon®

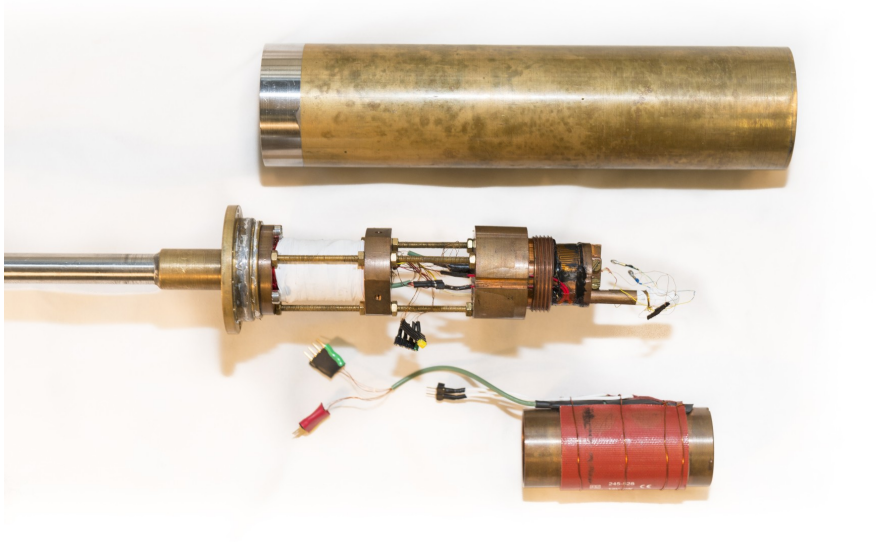

Figure 2.3.: Sample holder centrepiece with radiation shield and vacuum cup

In figure 2.4 details of the sample holder head are discernable: figure 2.4a shows the head's 'front' with the sample retainer, while figure 2.4b pictures the 'back side'. On the front side, the screw-driven chuck for holding the sample is clearly visible (but no sample is mounted). In the very front of figure 2.4a the two thermocouples that get attached at a sample are apparent, the third thermocouple sits in its place in the sample holder between the screws holding the chuck. The yellow chromel thermocouple wires and the wires leading to the current source are anchored again at the pipe appendage for thermal and organizational reasons. The heater foil wound around the head (also called 'base heater') is visible right in front of the screw thread

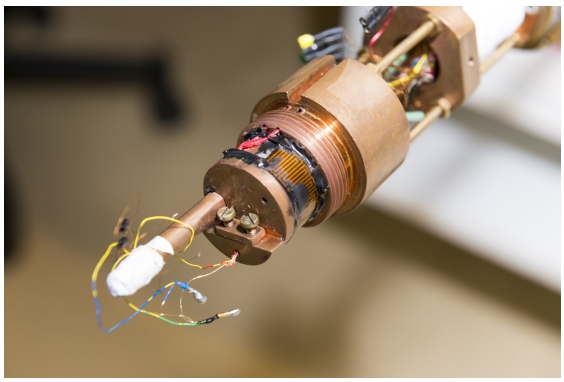

(a) Sample side

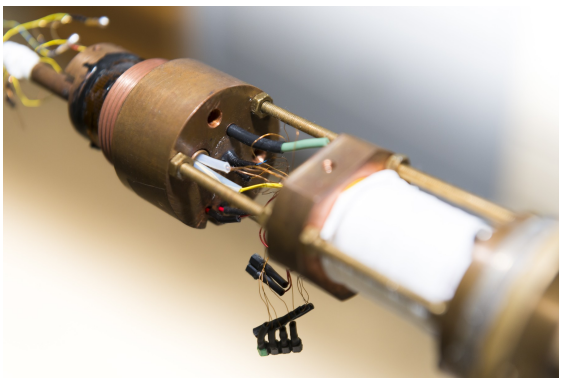

(b) Backside with sensor inlets

Figure 2.4.: Sample holder head

that allows mounting the radiation shield.

On the back side the temperature sensors' leads can be seen protruding from the sample holder, they are encased in heat shrink tubes. The Cernox™ sensor is placed directly in the centre of the head, the Pt-100 is located slightly off-centre, in figure 2.4b seen shifted to the top of the picture. The wires leading to the thermocouples and the sample heater are viewable entering the pipe appendage.

For details of the design of the sample holder and constructional drawings, see appendix A.

2.2.2. Temperature Sensors

A total of four temperature sensors were used in the set-up at hand – each a Pt-100 and a Cernox™ sensor for measuring temperatures of both the head (for getting a base temperature for the measuring process) and of the radiation shield (for controlling purposes and minimizing thermal radiation errors). A set of two sensors each is used, because neither sensor satisfactorily covers the whole intended temperature range (from below the boiling point of helium up to room temperature). The Cernox™ sensors are used for temperatures up to 50 K, above that the Pt-100 sensors take over.

Both kinds of temperature sensors are connected via thermal grease to their respective mounting points to ensure good heat exchange – necessary for keeping the sensor at same temperature as the sensed object. In case of the radiation shield, they are pressed to the outer side of the shield with a thin film of thermal grease in between to guarantee an optimal thermal coupling and they are being held in place by heat shrink tubes and the wires also responsible for holding the heater mat in place. In case of the head, two holes are drilled, so that the sensors can be placed inside the head, as close as possible to the end near the sample.

Pt-100

Pt-100 temperature sensors are resistance temperature detectors with platinum as the sensing element (hence the 'Pt') and a resistance value of 100 Ω at a temperature of 0 °C (hence the '100'). Pure metals follow a relatively linear correlation between temperature and resistivity. Platinum, as a noble metal, offers good long-time stability and resistance to environmental influences. It also has the most stable temperature-resistivity correlation and a very good working range with regard to temperature. Hence Pt-100 sensors are well-established as standard in scientific and

industrial applications and their behaviour is well known and documented [10].

Cernox™

Cernox™ thin film resistance temperature sensors by LakeShore Cryotronics Inc. are ceramic oxynitride resistors made of sputtered zirconium thin films. The feasibility of using such materials as cryogenic thermometers has been shown in [11]. The process of developing and producing these thermometers was refined at LakeShore Cryotronics Inc. [12]. By sputtering a ZrN lattice in an atmosphere of argon, nitrogen, and oxygen and controlling the deposition parameters, the incorporation of oxygen into the lattice can be regulated. With increasing oxygen content the lattice enlarges and the electrical resistivity changes accordingly. Therefore the sensitivity of the sensors can be arranged to be optimal in a chosen temperature range, typically for very low temperatures.

As the Cernox™ sensors were not calibrated by the manufacturer, calibration had to be conducted locally. Calibration was performed at the helium-3 cryostat of the Institute of Solid State Physics in collaboration with Friedrich Kneidinger and Norbert Ackerl. With this cryostat, temperatures down to about 350 mK are attainable, which made it an obvious choice. The Cernox™ sensors were calibrated by gauging them against a known sensor by placing them as close as possible next to each other on a brass mount to ensure they are at the same temperature. A slow temperature drift from 350 mK leading up to 120 K allowed to get characteristic curves for the 'new' sensors. A similar calibration process (for verification purposes) was later on conducted in a helium-4 cryostat in co-operation with Herbert Müller. Modified sensor mounts for even better thermal equality between the sensors and a different reference sensor were used in this experiment.

The extensive calibration process yielded characteristic resistance curves for both Cernox™ sensors as shown in figure 2.5.

2.2.3. Heaters

Both the radiation shield and the sample holder base are outfitted with heaters to counteract the external cooling and therefore enable to maintain constant and fixed temperature levels. Extensive testing led to the conclusion that flexible heating pads surrounding the respective bodies lead to best behaviour.

For the sample holder head a flexible thermofoil heater – a resistive meandering heater inlaid in a thin polyimide film – is affixed in a groove in the sample holder

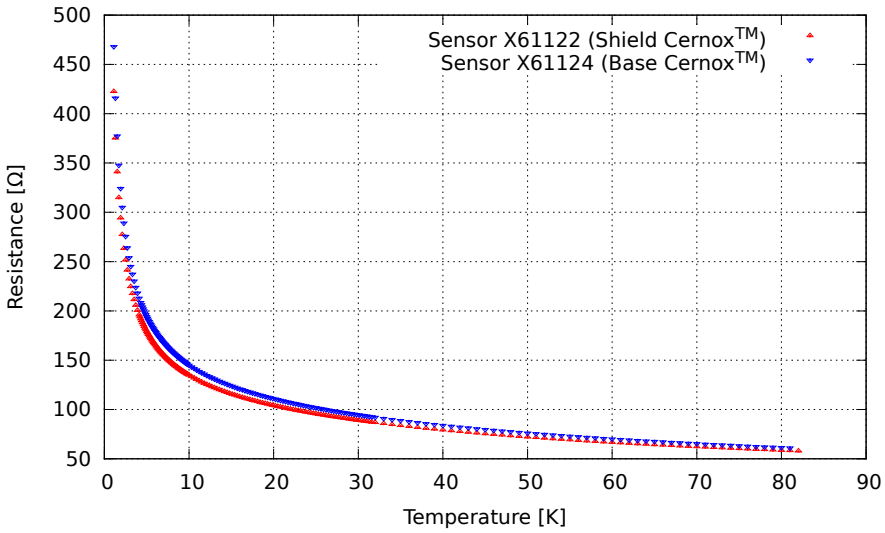

Figure 2.5.: Characteristic sensor resistance curves

head. The heater in case is an 18 Ω model HK 5215 thermofoil heater by Minco Products, Inc. [13]. Special attention has to be paid to thoroughly mount the heater on the head as the considerable heating power can damage the heater itself if the heat is not conducted uniformly into the massive copper block that is the sample holder head. Because simply pressing the heater onto the block and holding it in place by bands of PTFE has not proven to be sufficient, an adhesive has to be chosen that not only is a feasible thermal conductor at a wide range of temperatures but also resists repeated thermal cycling and does not lose its bonding properties even at cryogenic temperatures. Fitting these characteristics is the Stycast® 2850FT epoxy encapsulant by Emerson & Cuming, its properties are detailed in [14].

For the radiation shield, due to the bigger size of the heater and a reduced power demand, a much lower power density in the heater is sufficient. Therefore a simpler and cheaper silicon-embedded heater pad can be used. Its mounting can also be achieved by simpler means, the (in principle) self-adhesive pads are held in place by tapings of PTFE bands or copper wires, as the provided adhesive will not work satisfactorily in cryogenic environments.

2.2.4. Thermocouples

For measuring the small temperature differences along the sample (and between the sample and the base temperature) thermocouples are used. Due to the Seebeck-effect, two different metals will generate a voltage that depends on the temperature

of the junction (and the metals themselves).

As the accuracy of the absolute temperature's measurement is a rather delicate thing to achieve and the absolute values are not strictly necessary (they are measured by the Pt-100 or Cernox™ sensors), only temperature differences between thermocouples are measured. By short-circuiting two thermocouples, i.e. using one wire as part of the two-metal junction in two different thermocouples and using the same material as second part of the junction, the temperature difference of the two junctions directly translates into a voltage on the leading wires (see also fig. 1.1). Even as the occurring voltages are relatively small, by using a nanovoltmeter and the known correlation function it is possible to measure the temperature differences along the sample accurately. The connections to the voltmeter (and all intermediary connections) have to be at the same temperature in both threads to avoid measurement errors.

For cryogenic applications, thermocouples made out of chromel and gold/iron are known to have a very high sensitivity at low temperatures. Chromel is an alloy of 90 % nickel and 10 % chromium. Gold/iron denominates a gold wire with a small fraction of iron in it. In the design at hand gold wires with 0.07 atom percent iron are used. The properties of chromel-gold/iron thermocouples are well-known and well-used for a couple of decades now. [15]

For practical purposes, the thermocouples were soldered together and put inside a metal casing (for additional strength and ease of application at the sample). Once again, Stycast® epoxy was used to fix the thermocouple inside the casing, because of its excellent cold resistance and thermal conductivity. It also acts as electrical insulator between thermocouple and casing.

2.2.5. Wiring

The various sensors and heaters have to be connected to the measurement instruments. A variety of requirements are demanded of the wires used. For insulation, due to high flexibility and a comparatively small increase in diameter as well as high durability through repeated thermal cycling (down to cryogenic temperatures), PTFE-coated wires are chosen. Single strands of wire lead from the sampler holder's head up to the outlets in the vacuum flanges. According to the demands based on the wires function, different wire materials and diameters are used.

For the heater wires, low electrical resistivity is of importance due to the relatively high current to reduce Joule heating. Therefore copper wires with comparatively large diameters have to be used, even though they transfer a considerable amount

of heat into the sample holder head due to copper's good thermal conductivity.

The sensors and the strain gauge are all operated in four-terminal sensing mode. Therefore, for each sensor/strain gauge there are two current-carrying wires and two wires for measuring the voltage drop. The current leads are again made of copper, albeit with a smaller diameter as the heaters', since the current is much lower. For the voltage leads electrical resistivity is of no big concern, therefore they are made of phosphor bronze which has a fairly low thermal conductivity.

The thermocouple wires are made of chromel and gold/iron as mentioned in section 2.2.4. The gold/iron wires form only short connectors between the actual thermocouples. The chromel leads run all the way to the outlets to avoid having another junction of different metals (and therefore another thermocouple) at unknown (and worse, possibly different) temperatures.

For details on the wiring layout and connector configurations see appendix A.2.

2.3. Sample

The sample holder can accommodate samples of varying dimensions. The sample cross-section can be up to 3 mm by 4 mm – but does not have to be rectangular, the cross-section can be any shape, as long as it is constant along the length of the sample. A rectangular shape is still to be preferred as it eases mounting the sample between the sample holder's chuck jaws and calculating the cross-section (the latter part also holds true for a cylindrical sample). A sample with at least one flat surface (pressing against the sample holder) also improves the thermal contact between sample and sample holder, accelerating temperature equalization. The minimal cross-section is only defined by the sample's sturdiness – and the active area of the strain gauge used as a heating element. The length of the sample can be up to about 30 mm, the sample (and its connection wires) just have to fit into the radiation shield. The sample's minimal length is not as sharply defined. As the sample is held in place by a chuck on one end, sufficient length has to be 'sacrificed' to ensure a firm hold. Temperature is measured at two different points along the sample and the 'free' end is equipped with a strain gauge for heating purposes. The distances between these points can be varied, but measuring accuracy diminishes with decreasing distances.

Figure 2.6 shows a prepared sample of rectangular cross-section with the strain gauge heating element glued to one end and copper strands covered in solder acting as pick-ups for the temperature-sensing thermocouples.

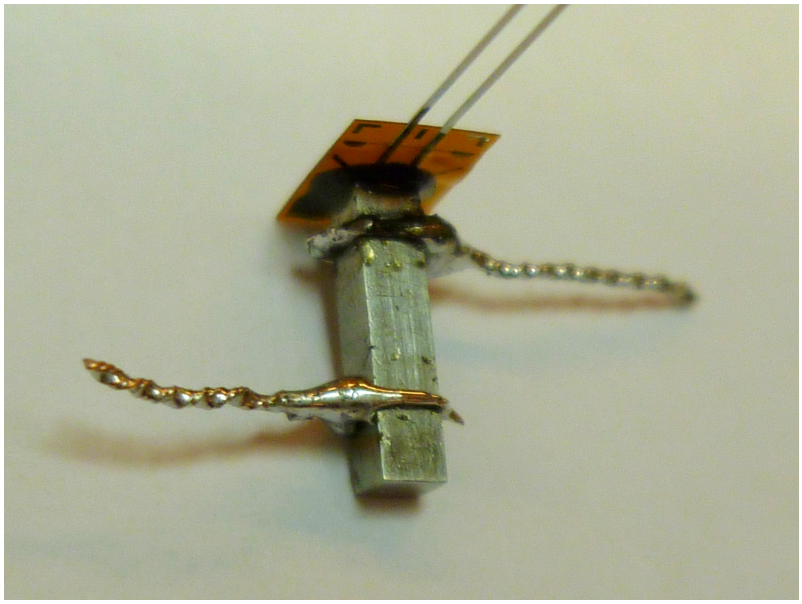

Figure 2.6.: Sample with added heater and temperature pick-ups

2.4. Hardware and Equipment

This section provides a short overview of the laboratory equipment and their respective uses in the set-up at hand.

2.4.1. Measuring Instruments

LakeShore Model 336 Temperature Controller

The LakeShore Model 336 Temperature Controller [16] is a central part of the measurement set-up. It monitors and controls the temperatures of the sample holder's base and radiation shield.

It possesses four sensor inputs supporting diode, resistance temperature detectors and thermocouple sensors alike. For standardized sensors response curves are already integrated, custom curves for each sensor can be supplied by the user as well. With appropriate sensors temperature ranges from 300 mK to 1500 K can be measured. Each sensor has its own current source, the excitation currents (1 mA for Pt-100 sensors, 30 µA or 100 µA depending on the temperature for Cernox™ sensors) are optically isolated from other circuits. The measurement resolution within the present temperature ranges lies at 2 mΩ for both Pt-100 and Cernox™ sensors.

For temperature control, two heater outputs with 100 W and 50 W power, respectively, are available. They are regulated by proportional-integral-derivative (PID)

controllers [17], the actual values of which can be defined separately for different temperature ranges.

The temperature controller is used for measuring and regulating the temperature inside the sample holder. Two pairs of each a Cernox™ and a Pt-100 sensor are coupled with the two heater loops (the 'weaker' heater loop 2 is connected with the radiation shield's heater).

Keithley 2401 Current Source

The Keithley 2401 Low Voltage SourceMeter® [18] provides the current for heating the sample via the strain gauge. It is a combination of a very stable and low-noise DC current source and a low-noise, high-impedance multimeter. It is capable of supplying a stable current – at a typical current of up to 10 mA the source accuracy is better than ±7 µA. Via 4-wire measurement the dropped voltage is measured as well, therefore the power consumption of the strain gauge can be monitored very accurately.

Keithley 2182A Nanovoltmeter

The Keithley 2182A Nanovoltmeter [19] measures the small potential difference between two thermocouples caused by the Seebeck effect due to the differences in temperature. It has two channels for low-noise, high-resolution voltage measurement. It is capable of resolving voltage differences down to 1 nV and 10 nV for channels 1 and 2, respectively. The peak-to-peak noise at this resolution is typically lower than 10 nV. The more sensitive channel 1 is responsible for measuring the temperature difference between the pick-ups on the sample, channel 2 for the difference between the colder sample pick-ups and the sample holder base.

2.4.2. Laboratory Equipment

Vacuum pumps

To eliminate measurement errors due to ambient gas in the sample holder assembly, the sample volume has to be evacuated. Measurements have shown that a residual pressure of 10^{-5} mbar or lower is sufficient to make influences of the residual gas negligible.

To achieve such pressure values, a two-stage pump array is used, a rotary vane pump is followed by a turbomolecular pump. A rotary vane pump is a positive displacement pump that – through repeated expansion and compression of the gas that

streams into the pump volume by means of a rotary slide – generates a depression in the pump volume that sucks residual air out of the sample volume and expels it into the environment. This creates a pre-vacuum for the turbomolecular pump. A turbomolecular pump consists of an array of angled turbine rotors and fixed stators. The rotors spin at a high frequency (up to 1000–1500 Hz) that accelerate the gas molecules they hit towards the outlet.

The equipment at hand achieves a vacuum of 10^{-6} mbar after a few minutes of pumping.

Cryostat

Cryostats are used for reaching and maintaining low temperatures in experimental environments. They are mainly constructed according to the same principle as Dewar flasks: two containers are built within each other, and are joined only at the top, separated by vacuum otherwise, to minimize thermal interaction between the inside and the environment.

For this set-up two different types of cryostats are used. One is a bath type cryostat, the outer casing of the sample holder dips directly into the liquid coolant (either nitrogen or helium). The other type is a continuous-flow cryostat, the coolant (helium in this case) is sucked through a valve into the volume containing the sample holder by an external pump. Due to the Joule-Thomson-effect the coolant is cooled even further, therefore temperatures below the coolant's boiling point can be reached. The valve is equipped with a heater in case the maximum cooling power is not desired.

Helium level meter

To measure the amount of liquid helium left in a cryostat a helium level sensor is used. The liquid helium acts as a cooling agent and is used up (but recycled through return circuits into the in-house helium liquidizers).

The liquid helium sensors works by measuring the resistance of a superconducting wire (Nb_3Sn in this case) with a transition temperature above the boiling point of liquid helium. The part of the sensor submerged offers no resistance, therefore the the total resistance is an indicator for the helium level of the cryostat.

2.5. Software

The measurement process is controlled by a computer, it is the centrepiece of the system. The various measurement devices are linked to the computer by GPIB (General Purpose Interface Bus, IEEE-488). They are embedded into the system via a socket server structure, as used in an increasing number of experiment set-ups at the Institute of Solid State Physics. Most of these structures were created by Herbert Müller from said Institute. The socket servers, as well as the measurement programs, are written in version 2.7 of the Python programming language [20]. With the exception of the socket server control program (which has a graphical interface), all programs are controlled by command line interface, so Linux is an advisable choice for the computer's operating system.

A short overview of the measurement process is given in the next section, a detailed operator's manual is found in appendix B.2.

2.6. Measurement

Once the measurement process is invoked by the proper set-up of the measurement's configuration files and the appropriate terminal commands, it processes automatically all defined measurement points. No further input from the user is needed (although it can be supplied to alter the measurement points or parameters). Only during exceptionally long measurements the coolant level has to be observed and the coolant topped off when necessary.

A rough sketch of the measurement process is depicted in figure 2.7. It will aid in the description of the process in this chapter, abbreviations used in the figure will be explained therein. Measurement begins after invoking the measurement program by entering `methecond.py <configuration_file>` into the configuration file. For detailed information on how to create the configuration file as well as advanced input commands, see the manual in appendix B.2.

In the first step, all measuring instruments and their socket servers are initialized and checked for connectivity; the configuration file's input is processed and the sensors are tested. Finally, files for documentation and logging purposes are created. When the system is ready for it, measuring commences.

For each measurement point, the process stays the same. The temperature controller is set to achieve the desired sample temperature. Depending on the temper-

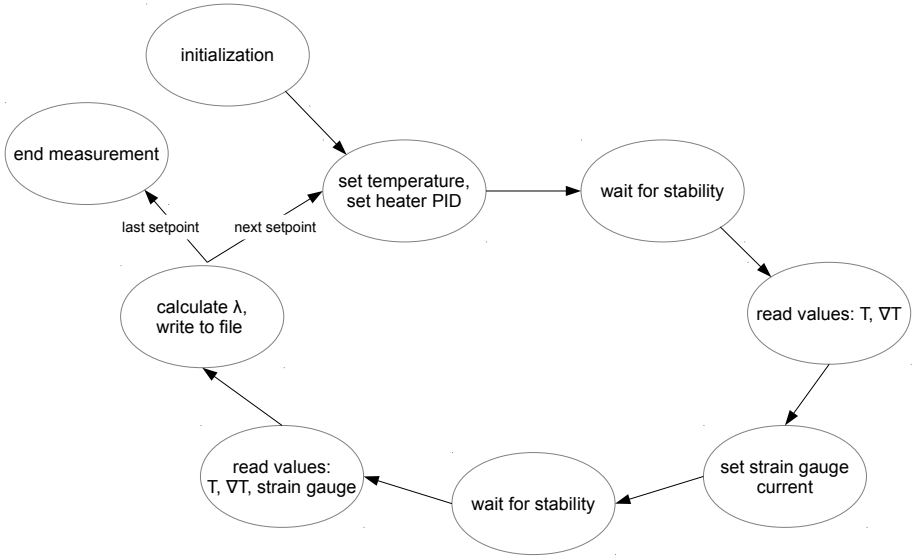

Figure 2.7.: Measurement process

ature either the Cernox™ or Pt-100 are chosen for measurement. The temperature set-point also defines the heaters' settings. For both the base and the radiation shield's heater separate PID and power values are allocated. A routine that periodically monitors and saves the values of the system's temperature and the temperature gradient along the sample is started.

To get reliable results, the system has to become stable. The temperature deviations are compared to the maximum accepted deviation as defined in the set-point's configuration – typical admissible tolerances are in the range of 0.02 K per 300 s. The temperature gradient stability is checked as well. It is defined in a fixed configuration file (called `methecond.conf`), and currently set at 0.003 K per 120 s. In the event that the desired stability cannot be reached, the measurement continues in any case after reaching a time-out (currently set at 60 minutes) in order to not freeze the whole measurement process. A measurement exception is added to the log file to inform that this measurement point may be compromised.

In the next step, the temperature values of sample holder base and radiation shield, and the residual temperature gradient along the sample are recorded and used as a baseline for the measurement. The Cernox™ or Pt-100 sensors and thermocouples are used for this, respectively. For enhanced accuracy, the thermocouple measurements are repeated multiple times and the mean value is taken.

For measuring thermal conductivity a heat flux has to be induced into the sample. This is achieved by heating one end of the sample by a glued-on strain gauge, 'misusing' it as an ohmic resistance heater. The heater power is set to a value, so

that the sample is supposed to have a temperature difference along the tap length of between 0.25 K and 2 K, depending on the base temperature. At first, reasonable heater power values are ballpark figures, but after each measurement the actual temperature difference between the pick-ups is compared to the desired value, and the heater power reference table is updated so that after few iterations the desired temperature differences can be achieved reasonably good.

After turning on the strain gauge heater, the system (especially the temperature gradient) has to stabilize itself once again. Typically this happens significantly faster than the initial stabilization, the time-out is currently set at 20 minutes.

For comparison, once again the measurement values of the temperature sensors and the thermocouples are recorded. This time, the current source's power data is read as well. The current is set (and known), and by 4-wire measurement the strain gauge's resistance value can be determined. This allows for a calculation of the strain gauge's power output.

Now all parameters for calculating the thermal conductivity of the sample at the current temperature are available. The calculation follows the principle shown in section 1.4, explicitly as expressed in equation 1.59 ($\lambda = \frac{\dot{Q}}{\Delta T}\frac{l}{A}$). The sample dimensions are known and it is a reasonable approach to assume that the entire heat from the strain gauge flows into the sample and therefore equate the strain gauge's power output with the heat flux through the sample. The temperature difference is received from the nanovoltmeter measuring the thermocouples, the zero-values obtained earlier are subtracted to minimize errors. Each measurement point is associated with a single temperature. The nature of the measurement requires a temperature gradient along the sample, hence only a mean temperature value can be given. A natural choice for this is the temperature of the sample midway between the temperature pick-ups. A good estimate consists of taking the sample holder's base temperature and adding the temperature difference between it and the lower pick-up (wherefore another thermocouple is placed at the sample holder's base) and half of the temperature difference between the sample's pick-ups.

All measurement parameters and calculation are then saved to the output files, the monitored temperature trends are saved to separate files as well for future reference. If there is another measurement point to be handled, new target temperatures and heater PID values are set and the process starts over.

If the last set-point is reached, the measurement program starts its shut-down sequence which handles the proper termination of all processes involved and double-checks that all heaters are turned off.

3. Results and Discussion

3.1. Limitations

3.1.1. Measurement Errors

Every measuring process is subject to errors that limit the accuracy and precision of the measurement. Hence it is important to shed some light on the most common sources of errors and on how to minimize them. For calculating the coefficient of thermal conductivity, equation 1.59 is used. The possible errors can be grouped thematically:

Geometry Even though the exact shape of its cross-section is irrelevant (as long as it is constant) for practical reasons a cuboid (or at least cylindrical) sample will be preferable. The dimensions can be measured relatively simply by using a calliper – with its own measurement errors. Considerably deviating results will be obtained if the sample does not have a constant cross-section. Not only can no reliable value for cross-section be set, with varying cross-section the heat flux density also changes along the sample and leads to systematic errors.

The second geometry-related factor is the length l, it is measured between the two temperature pick-ups T_H and T_L (as seen in figure 1.1). The pick-ups are made of copper strands, they naturally have a finite thickness. This length l can be defined as the centre-to-centre distance, but an exact measurement can be tricky at times. Special care has to be taken that the pick-ups are aligned parallel to each other and perpendicular to the sample. In case the pick-ups are not fixed sturdily enough, they can become loose and therefore alter the measurement to the point of uselessness.

Temperature Differences ΔT is measured via two chromel-gold/iron thermocouples. Even when following proven standards for thermocouple response curves [15, 16], deviations can occur as both chromel and gold/iron are alloys and inhomogeneities and concentration deviations can occur. In case of chromel they are neg-

ligible, but for the used gold/iron wire (with only 0.07 atom percent iron) small variations can have measurable effects [15].

Furthermore, as the thermocouple cannot be applied directly to the sample, the measured temperatures can deviate from the actual values. The pick-ups are constructed as copper strands wound around the sample (or even carefully soldered to it). They can therefore only register the mean surface temperature at a given point along the sample, a radial temperature gradient inside the sample is indetectable. As the thermocouple has to be electrically insulated from the sample, it is incased in a small droplet of Stycast® and located inside a metal casing. All these materials (as well as the small length of copper of the pick-up itself) add up as thermal resistivities, therefore the measured temperature at the thermocouples can differ from the actual sample temperatures. But as only the temperature *difference* between the two points is of interest, it can be assumed that both points are affected to a very similar degree and therefore the error gets minimalized.

Heat Flux Getting an accurate estimate for the heat flux along the sample is not a trivial task. It will be assumed that all heat emitted by the strain gauge (acting as a heater) flows through the sample volume. In order to get a reasonable value for the heater's power consumption 4-terminal sensing is used. Although a small measurement error is induced by this, a small length of chromel wire separates the strain gauge from the lead wires – with its high thermal resistivity the chromel minimizes heat drain from the strain gauge into the lead wires.

Heat can also flow through the wires from the outside (at room temperature) into the measurement volume (and then into the strain gauge or the thermocouples and therefore into the sample). To alleviate this, the wires are thermally anchored at the base of the sample holder, i.e. they are wound several times around it to align with its temperature. Chromel offers a relatively low thermal conductivity [21] ($\lambda \approx 17\,\mathrm{Wm^{-1}K^{-1}}$ at room temperature), which further lessens the issue. The voltage-sensing wires can be made of high thermal resistivity wire (high thermal resistivity is coupled via the Wiedemann-Franz law with high electrical resistivity) because next to no current runs through these wires and therefore the ohmic losses are negligible. For the current-carrying wires copper wires have to be used to reduce the ohmic losses.

Any residual gas in the measurement chamber will also contribute to thermal conductivity. As its influence is proportional to the amount of gas (or its pressure) the use of a vacuum pump will greatly diminish the measurement error. By using

a turbomolecular pump, vacuum up to 10^{-6} mbar can be reached and the impact of residual gas heat transfer becomes negligible.

All bodies with finite temperature emit electromagnetic radiation (black-body radiation) whose spectrum and intensity depends on the temperature. According to the Stefan-Boltzmann law the emitted energy across all wavelengths is proportional to the fourth power of the temperature. Therefore, the importance of radiation interferences rises considerably with rising sample temperatures. To minimize heat exchange with the surroundings the sample is ensheathed in a copper *radiation shield* that is held (via a separate heater) at a temperature ideally identical to the sample temperature. Nevertheless, thermal radiation along the sample can amount to a considerable deviation when measuring thermal conductivity, especially at higher temperatures.

Sample Even if the measurement set-up worked perfectly and all errors were negligible, one still has to consider the quality of the sample. Little impurities and imperfections, as well as cracks or lattice defects (in crystals) can severely impact a sample's properties.

Absolute Temperature The aim for each measurement is to get a curve of thermal conductivity of a sample over varying temperatures. But it is not trivial to designate a distinct temperature: Due to the measuring principle a temperature gradient has to be applied to the sample, thus only a mean temperature can be stated. As stated in section 1.4, a good approximation for a median sample temperature can be derived by adding a third thermocouple to measure the temperature difference between the sample holder and one measurement pick-up. Since by design the temperature sensors in the sample holder are not in exactly the same location as this additional thermocouple, small deviations in temperature are possible. To ensure reliable results over a vast range (from single-digit temperatures up to room temperature) two different sensors are used: a Cernox™ for low values up to 50 K and a Pt-100 above.

The Cernox™ sensors used for measuring temperature at the sample holder base and the radiation shield were uncalibrated and therefore had to be calibrated in house. The Pt-100 sensors follow a standard response behaviour, testing procedures confirm this.

Calibration errors can occur if the to-be-calibrated and reference sensors are not at exactly the same temperature. Of course, each calibration deviation of the reference sensor transfers itself onto the new calibration. Although the reference sensors are

in use for some time already, fortunately Cernox™ sensors feature a good long time stability. Analyses [22] show that over a 5.8 year test cycle, the average calibration offsets are less than ±0.02% of temperature below 40 K.

3.1.2. Temperature Limit

The measurement assembly is cooled by liquid gases. Common choices are nitrogen and helium, their boiling points at standard pressure are at 77.4 K and 4.2 K, respectively. Without further preliminaries these are the theoretical lower limits to the temperature range. Further cooling is possible by lowering the pressure of the cooling agent (by applying a vacuum pump). The boiling point of the residual liquid decreases, due to the lowered pressure. The cryostat and pump at hand can realize temperatures down to about 1.5 K.

In reality the present set-up unfortunately does not stabilize at temperatures below approximately 12 K. Even though several measures have been taken, a residual heat input cannot be prevented and may exceed the cooling power at low temperatures. The voltage-sensing wires of the strain gauge heater have been replaced by phosphor bronze wires. All wires are thermally anchored at the base of the sample holder assembly, near the point where it is in contact with the coolant. Even some thermal bridges made of copper have been designed to connect the sample holder better to the low temperature base (due to better mechanical properties, the supporting structure is made of brass).

Cooling the assembly with residual gas present allows the sample holder to reach the temperature of the liquid coolant, but subsequent evacuating (necessary for correct measurement, see section 3.1.1) reduces the cooling power to the point that it is insufficient to counter the heat input at low temperatures. Even though the warming process runs slowly (about 40 to 200 mK per minute) it is enough to interfere with the measurement and to prevent accurate results below about 12–15 K.

3.2. Results and Outlook

The measurement set-up in its present state represents a measurement device with a sound measurement principle and reproducible results. It is able to measure thermal conductivity of various solid samples from temperatures of about 15 K up to room temperature. It presents an easy-to-use measurement routine, that is self-operating once the starting conditions are set. The accumulating data is well documented

– lots of different measurement values and parameters are saved. The recording of the occurent temperature trends allows for easy diagnostics in case of problems and a feasibility-check of data points. Absolute measurement values are still to be considered cautiously, especially at higher temperatures, as the calibration process is not quite concluded.

The real question will be whether the problems at cold temperatures are solvable with this kind of layout (an externally cooled vacuum cup surrounding the measurement volume) or if a complete redesign is necessary where the coolant has a more direct interaction with the sample holder (for example by flowing through pipes inlaid into the sample holder's base).

Future enhancements

The most pressing objective in enhancing the set-up at hand lies in extending the measurable temperature range down to the limit imposed by the cooling agent. Possible sources of heat flux into the measurement volume have to be detected and counteracted. It has to be determined whether it is possible to eliminate enough of the heat input that the cooling is sufficient.

Extended temperature probing can help to identify which parts of the sample holder reach the lower temperature limit and which parts stay *warm*. By placing temperature sensors on different parts of the sample holder and cooling and evacuating the system the temperature distribution can be determined. For these testings the radiation shield can be disconnected, its sensor wires can be used.

In case that the wire anchor is cold, but the sample holder head is not, the cooling power would seem to be sufficient, but the thermal conductivity of the threaded brass rods connecting the anchor with the head is too low. Therefore copper *cold bridges* have to be constructed and used. The anchor part has already been prepared by slanting off some edges and drilling threaded holes. The sample holder head currently has no such preparations.

In case that the wire anchor is *warm* as well, either the thermal connection of the vacuum cup's (brass) top to the copper anchor is not good enough or too much external heat is entering the sample holder – in which case the source of the heat flux has to be identified and (in possible) minimized or eliminated.

Thermal radiation from the sample holder's top could be a source and radiation shields could be built into the connection pipe, but because of the length and small diameter of the pipe, the solid angle for actually reaching the measurement volume is quite small. Furthermore the connection pipe is filled with all the wires and encasing

PTFE tubes, effectively blocking the better part of direct radiation exchange.

Further redimensioning of the sample holder's wiring could prove to be an viable approach. The thermal sensor's voltage leads could be replaced by phosphor bronze, thinner (copper) current leads have to be considered as well. By far the thickest (and therefore most conductive) wires are the heater leads. Earlier attempts with thinner wires lead to meltings, but since then the heaters have been replaced with lower-powered ones, so there could be potential for redimensioning.

If all else fails, the inclusion of *cold fingers*, bridges that directly connect the sample holder's head to the vacuum cup's inner surface, has to be considered. Construction and operation are challenging though, as the vacuum cup narrows at its top, some sort of movable mechanism has to be devised. At higher temperatures such a cold finger could increase the coolant consumption considerably, as the warm sample holder head is then permanently (indirectly) connected to the coolant. In a worst case scenario, this additional cooling power could prove too much for the heater's ability to warm up the sample holder head.

In an attempt to reduce the heat input through the lead wires as much as possible, these wires are thermally anchored at a copper block directly connected to the vacuum cup, so that they are (presumably, but not proven) close to the boiling temperature of the coolant. For optimal measuring, the sensors' lead wires should be brought to the same temperature as the sensors to avoid unwanted heat flux. Another thermal anchor at the sample holder's base could achieve this for the thermal sensors. The strain gauge and thermocouple wires are already anchored again at the pipe leading through the sample holder head.

The calibration process is not entirely finished yet. When comparing the measurements of standardized samples with reference measurements, at higher temperatures deviations are noticable. A calculation routine to account for linear and quadratic corrections has been implemented but satisfying coefficients are still missing as a planned reconstruction to address the problems at very low temperatures is likely to alter these coefficients.

The Cernox™ sensors used in the set-up are not fully optimized for the intended temperature ranges. They are of the Cernox™ CX-1010 type which has its maximum of sensitivity well below 1 K, a temperature never reached with this set-up. A considerable increase in measurement sensitivity could be achieved by switching to a

CX-1050 type, or even a CX-1070 type if temperatures below 4 K are of no concern at all, see figure 3.1. The CX-1070 sensor would have the advantage of maintaining a reasonable sensitivity up to room temperature, therefore eliminating the need for the Pt-100 sensors and their corresponding (heat-conducting) measuring wires.

For reliable temperature measurements, the calibration process has to be refined to guarantee that the 'new' sensors and the ones they are compared with are veritably at the same temperature. A monetarily more sumptuous solution would lie in purchasing pre-calibrated ones.

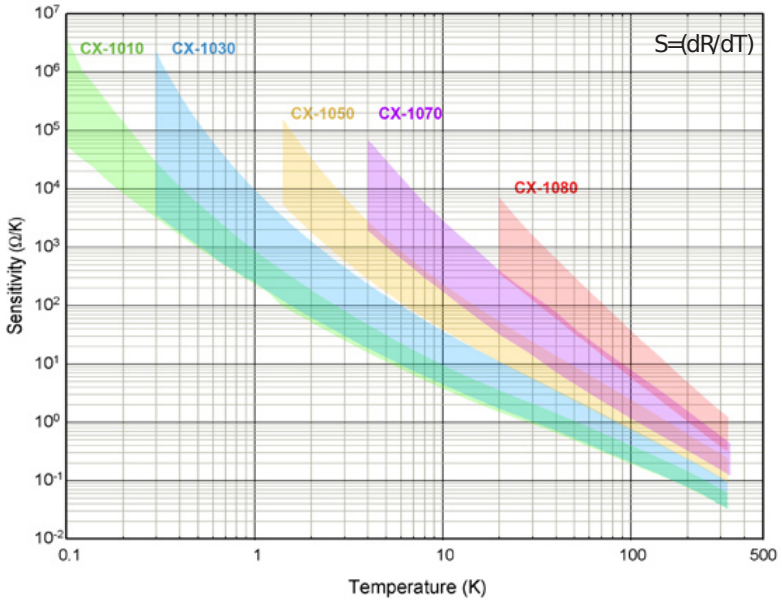

Figure 3.1.: Sensitivity comparison of different Cernox™ sensors [23]

A. Construction Details

A.1. Construction Plans

This section shows the constructional drawings of two main parts built for the sample holder, the sample holder head and the thermal anchor, followed by photographs and an exploded assembly drawing of the sample holder. The drawings were made with Solid Edge by Siemens PLM Software, the parts then manufactured by the workshop of the Institute of Solid State Physics, but sometimes altered thereafter to accommodate the continuous improvement process.

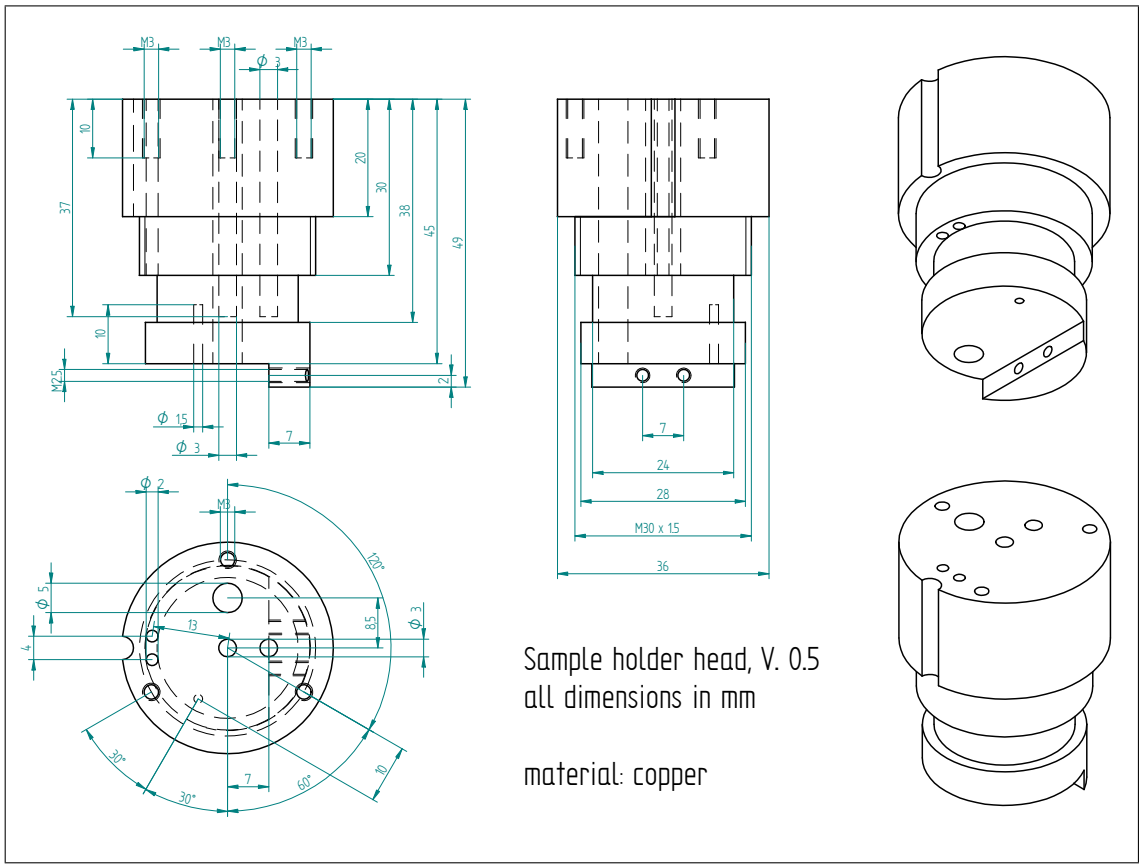

Figure A.1.: Constructional drawing of sample holder head

Figure A.1 shows the constructional drawing of the sample holder head. Later additions (not shown in figure A.1) are two holes (4 mm diameter and 15 mm deep) drilled into the base of the sample holder head to accommodate copper rods acting as thermal bridges, remnants of an intermediate design to ameliorate thermal conductivity between an older-design thermal anchor and the sample holder head. A further hole has been drilled into the very bottom part to allow the thermocouple sensing the base temperature to be located further from the base heater. It is drilled in between the threaded holes made for the screws holding the sample-fixating chuck in place (but perpendicular to it).

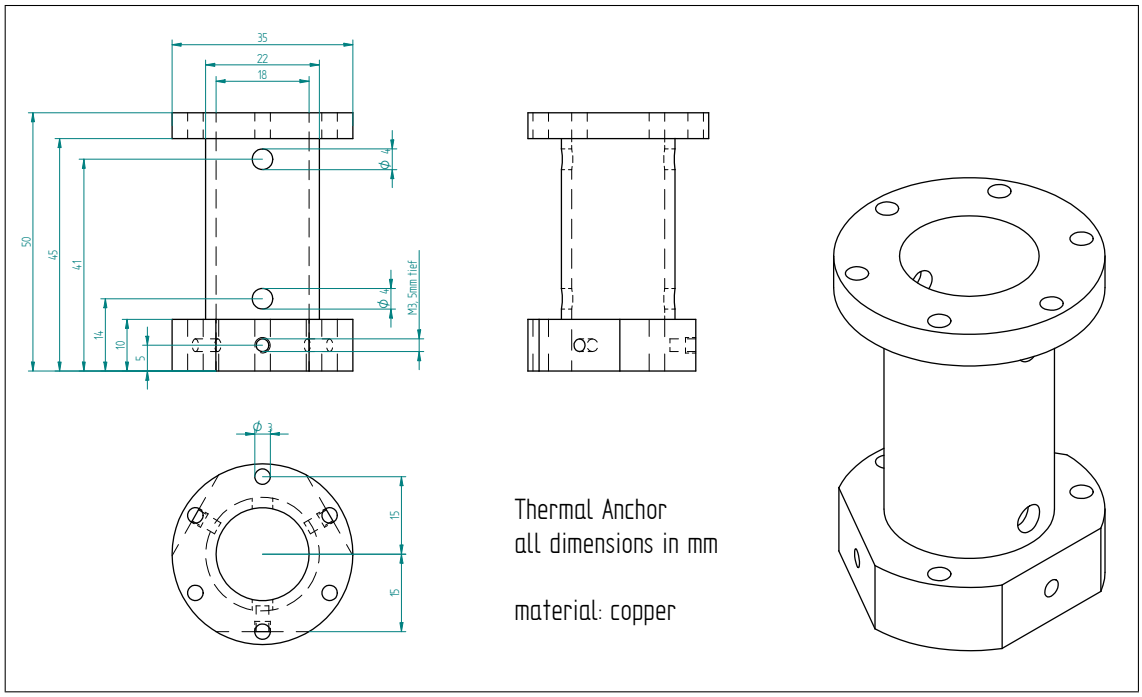

Figure A.2.: Constructional drawing of thermal anchor

The constructional drawing of the thermal anchor is shown in figure A.2. On the one hand it serves as a structural part – connecting the sample holder head (via threaded rods) to the whole assembly, as it is screwed directly to the vacuum cup's top (which in turn is welded to the connection pipe). On the other hand – as the name implies – it serves as a heat sink for the wires that lead down from the sample holder's top. Its direct connection to the vacuum cup enables it to cool down the wires wound around it, therefore reducing the heat flux along the wires into the measurement volume.

Figure A.3 depicts photographs of the sample holder. In figure A.3a the sample holder can be seen prior to any sample mounting, the separate constituents being

clearly visible. Figure A.3b shows the finished assembly, albeit without the vacuum cup. The radiation shield with its red silicon heater mat is standing out in the foreground.

An exploded assembly drawing of all parts comprising the sample holder up to the connecting pipe (but without any wires, screws or nuts) is shown in figure A.4. Marked in green are threaded parts, the positions of the heater mats are labelled in red; the sample is coloured black. All other parts are coloured copper, brass or steel grey, due to the material they are made of.

For reasons of clarity, in both figures A.3 and A.4 the vacuum cup normally surrounding the assembly is omitted as it would obstruct the view to more essential parts.

(a) 'Open' sample holder without sample (b) Finished assembly, without vacuum cup

Figure A.3.: Detail pictures of the sample holder

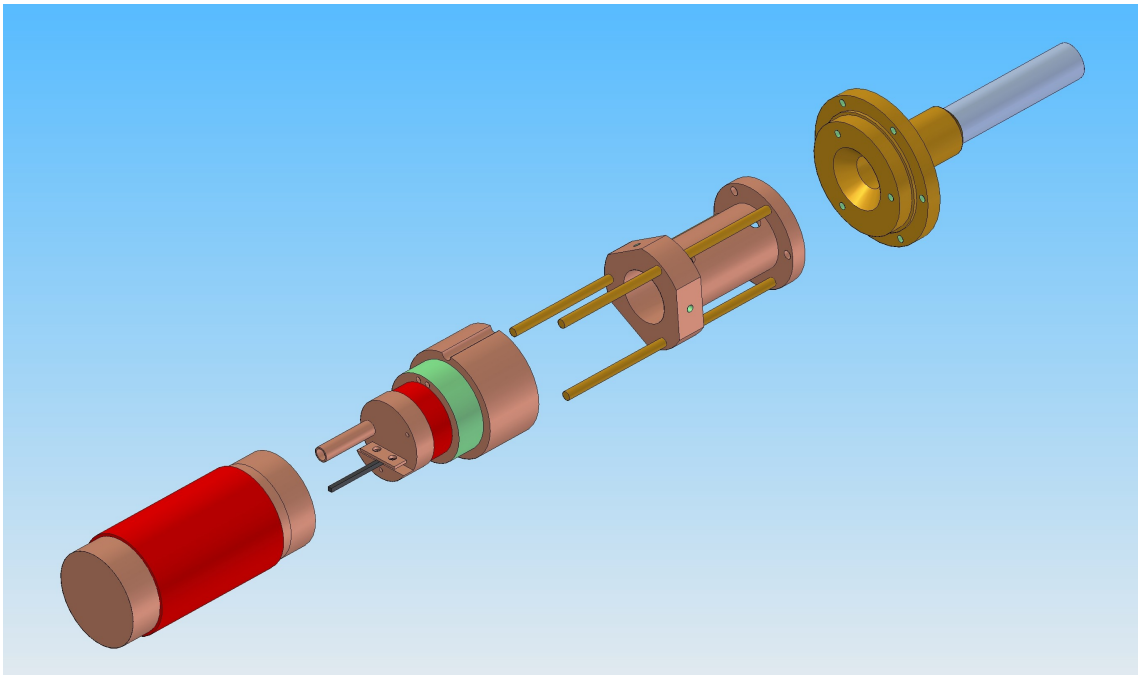

Figure A.4.: Exploded assembly drawing of the sample holder

A.2. Wiring Details

This section describes the wires and cables used and the pin layout of the connectors used.

A total of 27 wires lead up from the sample holder head through the connection pipe up to the top plate, where they are fed through to three vacuum-tight plugs by Fischer Connectors. From there, three connector cables lead to the measurement instrument – two cables to the temperature controller, one cable splits its wires between the current source and the nanovoltmeter.

Each of the four temperature sensors has four leads (for four-terminal sensing). The two heater pads are connected by two leads each, the strain gauge operates in four-terminal sensing mode, too. The last three wires are the chromel parts of the thermocouples leading to the nanovoltmeter.

Throughout the set-up, a colouring scheme to avoid confusion has been implemented. Whenever possible, parts belonging to the radiation shield are coded red, parts belonging to the sample holder base are coded blue. If connections to different sensors are necessary, distinctions are made in green and yellow: Pt-100 are marked green, Cernox™ yellow.

Figure A.5 shows the pin configuration of the 11-pin vacuum-tight Fischer 104 Z 056 plugs and receptacles. The top part (just above pin 10) is marked with a little

red dot both on the plug and the receptacle to ease the fitting. The orientation of the connector in question has to be borne in mind – when looking at the backside (e.g. when soldering), the layout appears mirrored.

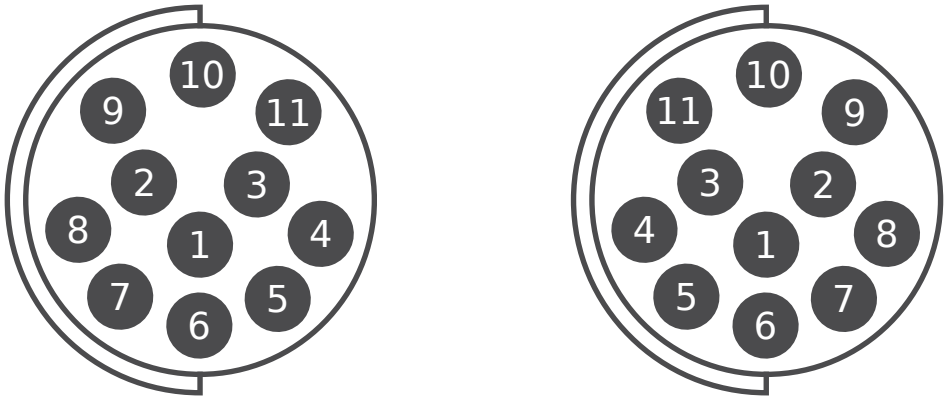

(a) Panel-mounted plugs, pin view; cable-mounted receptacles, solder view

(b) Cable-mounted receptacles, pin view; panel-mounted plugs, solder view

Figure A.5.: Pin configuration of Fischer 104 Z 056 connector

The three connectors are grouped thematically and are colour-coded to avoid confusions. The red-coded receptacle and cable are assigned to the temperature sensors and heater of the radiation shield, the blue-coded receptacle and cable to the sensors and heater of the sample holder base; the unmarked receptacle and the black-coded cable are assigned to the strain gauge and the chromel thermocouple wires. Each cable is composed of ten wires – leaving one pin each unconnected; each wire insulation is coloured differently. Table A.1 lists all cables and plugs used, their pin configuration and what colour wire in the cable it connects to. For each lead in a four-terminal sensing, its function, whether current-carrying or voltage-sensing (I or U, respectively), as well as the polarity are noted in column 'function'.

On the temperature controller's backside, a 6-pin DIN 45322 socket is used for each sensor. Each of the 4 connectors has its colour-code painted on to link it to the correct input (e.g. red-yellow for the radiation shield's Cernox™ sensor). Inputs from left to right correlate to base Cernox™, base Pt-100, shield Cernox™ and shield Pt-100. The pin assignment of these DIN connectors are found on page 33 of the temperature controller's user manual [16]. Next are the connectors (two banana plugs each) for the heater pads – the base heater is labelled 'heater 1', the shield heater is 'heater 2'.

The three chromel thermocouple wires lead to the input of the nanovoltmeter. As both the voltage between the *warm-* and *cold-* side thermocouples (T_H and T_L in

Colour code	Pin number	wire colour	connected element	function
blue	1	n/a	disconnected	n/a
blue	2	purple	base heater	+
blue	3	black	base heater	-
blue	4	yellow	base Pt-100	U+
blue	5	grey	base Pt-100	I+
blue	6	pink	base Pt-100	I-
blue	7	blue	base Pt-100	U-
blue	8	red	base Cernox™	U+
blue	9	white	base Cernox™	I+
blue	10	brown	base Cernox™	I-
blue	11	green	base Cernox™	U-
red	1	n/a	disconnected	n/a
red	2	purple	shield heater	+
red	3	black	shield heater	-
red	4	yellow	shield Pt-100	U+
red	5	grey	shield Pt-100	I+
red	6	pink	shield Pt-100	I-
red	7	blue	shield Pt-100	U-
red	8	red	shield Cernox™	U+
red	9	white	shield Cernox™	I+
red	10	brown	shield Cernox™	I-
red	11	green	shield Cernox™	U-
black	1	purple	none	none
black	2	grey	none	none
black	3	black	none	none
black	4	white	strain gauge	U-
black	5	green	strain gauge	I-
black	6	n/a	disconnected	n/a
black	7	yellow	strain gauge	I+
black	8	pink	strain gauge	U+
black	9	blue	thermocouple T_H	
black	10	red	thermocouple T_L	
black	11	brown	thermocouple T_B	

Table A.1.: Fischer 104 Z 056 pin assignment

figure 1.1; measured in channel 1) and the *cold* and base-mounted thermocouples (T_L and T_B; measured in channel 2) are of interest, one wire has to be split in the plug fitting into the nanovoltmeter. A custom-built LEMO 2182-KIT connector is used in the connection – the pin assignment is detailed on page 2-13 in the nanovoltmeter's user manual [19].

The current source is connected by plain banana plugs, coded red and black for positive and negative terminals.

B. Operating Manual

B.1. Assembly

Sample assembly starts with mounting the temperature pick-ups (presuming the sample itself has already been obtained and cut to size). For this purpose it has been found to be advantageous to wind thin copper strands around the sample to create the pick-ups. For further fixation on metallic samples, these strands can be soldered carefully to the sample. Spot-welding could also be used for this purpose, but in practice has turned out to be intricate, as the current tends to run along the copper strands and not into the sample. Other bonding mechanisms are also possible, but one should always aim for maximum thermal conductivity between sample and pick-up. A few centimetres length of wires should be left standing away, so that the thermocouples can be soldered to them.

The strain gauge that acts as a heater to achieve a temperature gradient has to be fixed on one end of the sample, preferring the one with the 'cleaner' surface for better adhesion and heat transfer. The glue has to withstand not only temperatures down to the boiling point of helium but also repeated thermal cycling and rapid temperature changes, as the strain gauge has a considerable power intake. Once again, Stycast® can be used, however, simple super glue will also work (since its poor thermal conductivity is not of consequence here). Attention has to be paid that the strain gauge's active area is placed directly on top of the sample to ensure proper heating and prevent damage to the strain gauge.

The sample can then be fastened to the sample holder by placing the free end between the chuck jaws and tightening the screws. The thermocouples are soldered to their respective pick-ups at the sample – as close as reasonably achievable to the sample to get an accurate measurement. They are colour-coded so that they are soldered to the right position: blue goes to the *warm* end of the sample (near the strain gauge), green to the *cold* end (near the head). The red-coded thermocouple should already sit in its hole drilled into the base (and stay there). In case the colour-

codes get rubbed off (or no comparison table is available), it is to be noted, that the thermocouple on the *cold* side has three leading wires, as it sits in the middle and is part of two differential measurements and the base-thermocouple should be free of solder residues. Soldering with low temperatures is recommended as higher temperatures can potentially damage the thermocouples.

The two leads of the strain gauge (after shortening, if appropriate) are soldered to their respective pair of wires (for four-wire sensing). Care has to be taken, that the uninsulated leads of the strain gauge can not get into contact with the conductive radiation shield, once it is put on. Careful bending into shape of the wires or covering them with insulating tubes can prevent contact.

After screwing on the radiation shield, its instruments can be connected by plug connectors. They are colour-coded as well: the four-pin connector and its receptacle for the Cernox™ sensor are coded yellow, for the Pt-100 they are coded green. The heater only has two leads, mix-up with the sensor leads is therefore ruled out; the polarities are of no concern. At this point, controlling all connections by measuring the respective resistance values and checking them for reasonability is – while not strictly necessary – firmly recommended.

A basic guideline of common resistance values at room temperature, when measured directly at the pins of the connector plugs at the sample holder's top plate:

- between any two thermocouple contact pins (blank connector, pins 9, 10 and 11): about 195 Ω
- strain gauge, along one 'leg' (blank connector, pins 4 & 5 or 7 & 8): about 30 Ω
- strain gauge, at 'current' pins (blank connector, pins 5 & 7): about 150 Ω
- strain gauge, at 'voltage' pins (blank connector, pins 4 & 8): about 173 Ω
- any temperature sensor, along one 'leg' (red *or* blue connector, pins 4 & 5, 6 & 7, 8 & 9 or 10 & 11): about 45 Ω
- any Pt-100 sensor, through the sensor (red *or* blue connector, pins 4 & 7 or 5 & 6): about 154 Ω
- base Cernox™ sensor, through the sensor (blue connector, pins 8 & 11 or 9 & 10): about 77 Ω
- shield Cernox™ sensor, through the sensor (red connector, pins 8 & 11 or 9 & 10): about 75 Ω

Assembly is finished by putting the vacuum cup over the whole sample holder head and fastening it. Vacuum-tightness is achieved by applying Indium as gasket mate-

rial. A small length of Indium is placed inside a groove near the top; by pressing the cup against the device and screwing it tight, the indium gets squeezed and seals the connection.

After sample preparation and assembly the sample holder has to be inserted into a cryostat. A total of three cables have to be connected to the plugs in the top plate. As all three cables use the same type of connector, the connectors and their associated plugs are colour-coded. Two cables (with blue and red markings, connected to the blue and red plug, respectively) lead to the temperature controller, the black marked cable (connected to the last, unmarked plug) leads to the nanovoltmeter and the current source.

After connecting a vacuum pump to the ISO-KF flange, the ambient air can be extracted from the vacuum chamber. Residual moisture in the air could freeze out in the low temperature environment and disturb the measurement process, therefore evacuation is advisable to happen before cooling. As using a turbomolecular pump at ambient pressure can damage the pump, it has to be ascertained that a suitable pre-vacuum is generated using the rotary vane pump only. When the cryostat is filled with liquid coolant and the sample holder cooled down to the desired temperature the system is ready for measurements. For speeding up the cooling process, the measurement volume can be filled with an 'exchange gas' – a gas that enhances the temperature exchange rate between the vacuum cup (at the coolants boiling temperature) and the sample holder. A suitable choice for the exchange gas is to take the same gas that is used as the liquid coolant. Hereby it is ensured that the exchange gas cannot freeze out.

B.2. Measurement Software

B.2.1. Overview

The measurement devices are connected to each other by a standard General Purpose Interface Bus (GPIB, or IEEE-488). The communication occurs via a socket server structure and a central measurement computer unit. These socket programs are written in the 2.7 version of the Python programming language (for more information on Python see [20]). Sockets represent standardized interfaces for communication between two systems. Data is processed in a First-In-First-Out (FIFO) fashion, it is queued in a pipe. The operating system administrates all these sockets and allows

applications to interact with the measurement devices.

These python scripts run natively in a Linux environment, which makes it an obvious choice for an operation system. For the set-up at hand the Ubuntu 12.04 LTS distribution was chosen, but ultimately the choice of the Linux distribution is of minor concern. The measurement directory is found in `/home/thecond/measure`, a listing of the subdirectories and their function is found in figure B.1.

```
measure ..................... measurement directory
├── bin ..................... socket server executables
├── conf .................... configuration files for each
│                             measurement
├── doc ..................... documentation and information
│                             files
├── etc ..................... socket server configuration
│   │                         files
│   ├── init.d ................ starting scripts
│   └── sensors ............... sensor response curve files
├── lib ..................... socket server libraries
└── var
    ├── data .................. measurement data
    ├── html .................. files for displaying current
    │                         measurement in a browser window
    ├── lock
    │   └── pid ............... PID for running sockets,
    │                         deleted when stopped regularly
    └── log ................... log files
```

Figure B.1.: Directory tree

B.2.2. Measurement Process

Most of the measurement is controlled by simple inputs into the command line interface. An exception is the socket server control program, which features a graphical interface. For all commands, it is assumed that the working directory of the Linux terminal is set to `/home/thecond/measure` – the working directory is set by typing `cd <directory_path>`.

First of all, the socket server control program has to be started. It is invoked by typing `server_control.py` into the command line. If preferred, it can also be started as a background process (therefore freeing the terminal for further input) by adding an ampersand to the end of the command (`server_control.py &`). A graphical representation of all available socket servers and their states will pop up

(see figure B.2). Right after starting, all servers should be in status 'stopped' and

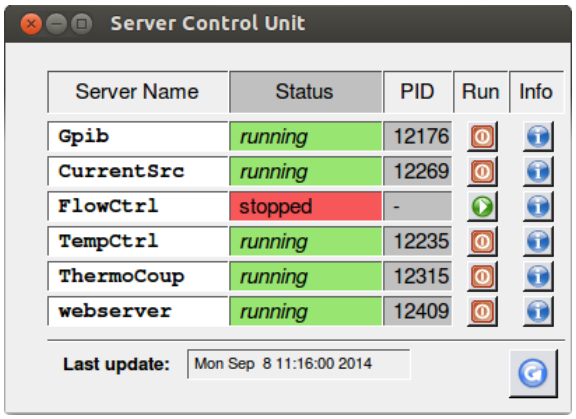

Figure B.2.: Socket server control program

no PID (process identifier, a unique number given to each running process by the operating system; not to be confused with the heater's PID – Proportional/Integral/Derivative – controller) should be given. Socket servers are available for the GPIB-interface ('Gpib'), the strain gauge heater current source ('CurrentSrc'), a temperature controller for the continuous-flow cryostat 'FlowCtrl'), the main temperature controller ('TempCtrl'), the nanovoltmeter reading the thermocouple voltages ('ThermoCoup') and a program for displaying the ongoing measurement in a browser window ('webserver').

Each socket server can be started by clicking the correspondent triangular 'play'-symbol. Stopping them can be achieved by clicking the 'poweroff'-symbol that appears when the server is running. Special attention has to be paid that the 'Gpib'-Server has to be started first, due to the fact that all measurement devices communicate by the GPIB system. Likewise, when shutting down the system, the 'Gpib'-server has to be stopped last. An exception to this rule is of course the 'webserver', as this socket does not rely on the GPIB system and is implemented locally on the measurement computer – therefore it can be started independently of all other socket servers.

When starting the 'Gpib'-server, a pop-up window asks whether the coolant is liquid nitrogen or helium. The reason for this lies in different heater parameters (due to different cooling effectiveness) and that in case of nitrogen cooling neither a helium-level meter nor the 'FlowCtrl'-server (for the temperature controller associated with the continuous-flow cryostat used with liquid helium) is used.

After successfully starting this (or any other socket server) the status switches to 'running' and the PID assigned by the operating system is shown (used for control-

ling and troubleshooting purposes). The starting button also changes to a stopping button. A small button labelled 'Info' yields further information for each server.

Alternatively, the socket servers can all also be started by command line – useful if operating in a remote environment. The starting command is `<socket>.py &`. Possible values for `<socket>` are `Gpib`, `CurrSrc`, `FlowCtrl`, `TempCtrl`, `ThermoCoup` and `my_webserver`.

When all socket servers are up and running the system is ready for measurements.

It is advisable to conduct a test measurement before starting the 'real' measurement to check for errors or wiring malfunctions. This can even be done before the assembly is inserted into the cryostat (or before the coolant has been supplied), the parameters are chosen to prevent overheating even without external cooling. The test measurement routine works with a severely reduced accuracy but therefore with a drastically improved speed and is typically finished in under 10 minutes. The test measurement is started by `test_measurement.sh` in a command line. Next, the geometry of the sample is asked (length between the taps and the cross-section in form of a breadth and width parameter), as well as the coolant type. After entering that, the measurement process will start and when it has finished, the results will be displayed in a browser window to allow a plausibility check by the operator.

For each measurement a configuration file has to be generated. A template for this can be found in the file `conf/sample_header.conf`. In this configuration file values for the operator (their name), saving directory and file names, a sample identification, geometry parameters, upper temperature safety limit and the coolant type have to be set. Lastly, the measurement parameters (defining at which temperatures measurements will be taken, as well as which level of stability has to be reached before an individual measurement will start) are to be entered. The syntax for these measurement parameters (prefixed by '`T=`' is defined as follows: a quintuple of values is equated with a set of measurements. For example '`T=A,B,C,D,E`' would relate to a series of measurements whose starting temperature set-point would be `A` K, then proceed in steps of `C` K until temperature `B` is reached. Each of these measurements would only start if the given temperature stability is reached: the deviation has to be smaller than `D` K over a time of `E` seconds. To allow for measurement series with decreasing temperature, `C` can also be negative. Multiple measurement series can be delimited by a semicolon (e.g. '`T=A1,B1,C1,D1,E1;A2,B2,C2,D2,E2`'). The

measurement set-point parameters can still be changed when the measurement is running.

The measurement itself is started by `methecond.py <configuration_file>`. After initialization the programs processes the list of measurement set-points one after the other (called *ranges* internally). For each set-point the programs runs through a loop of stages, as indicated in figure 2.7. Internally, these stages are called *states*, range and state can be changed manually, though should be done judiciously.

States `0`, `-1` and `-2` represent states of shut-down processes. State `0` is entered if the last measurement set-point has finished and the program shuts down properly. State `-1` is reserved for closing the program due to errors encountered. All measurement devices and procedures are set to a 'safe' state, all heaters are de-powered. State `-2` is only invoked by manually sending a '`QUIT`' command – only the current source for the strain gauge is de-powered, apart from that the system is left untouched.

The system tries to reach the temperature set-point defined in the configuration file. The appropriate commands to the temperature controller and the monitoring procedures are invoked in state `10`. State `15` comprises of a waiting period, long enough to accommodate the minimal time defined in the stability criterion for the set-point. In state `20`, a periodical check for stability occurs.

During states `15` and `20` the temperature controller regulates the heaters' power until the defined stability criterion is reached – the heaters' power and the cooling power are in equilibrium. Likewise the temperature gradient and its stability along the sample is monitored. The current temperatures are saved every ten second, the trend line can be viewed in a browser window at `localhost:8000/tcond/index.html`. If both the base temperature and the sample's temperature gradient are stable, state `30` is entered. If for some reason stability does not occur, measurement commences after a waiting period of one hour nonetheless, so that the measurement process does not get stuck up on a single measurement point. Accordingly, this 'error' in measurement is recorded in the output file and state `30` in entered regardless.

The current source powering the strain gauge gets switched on with an audible beeping noise and the sample gets heated up by the strain gauge placed on one end of it. The appropriate current value to achieve the desired temperature difference of 0.25 K to 2 K between the tap length on the sample (depending on the sample temperature) is sent to the current source. At first (for the first measurement points), a ballpark figure for this current value has to be used, as the temperature

difference generated by the current is dependent on the (yet still unknown) thermal conductivity of the sample. After each measurement, the current table is updated with measured values, quickly achieving the correct values to reach the desired temperature difference. The occurring temperature gradient along the sample is measured by the thermocouples at the taps.

In state `40` the program waits for the temperature distribution to reach a dynamic equilibrium. Once again, a time-out is provided in case this does not happen (raising again a measurement exception flag in the output file).

Once stability is reached, state `50` is entered – measuring and calculation. Thermal conductivity at the current temperature can be derived by applying equation 1.59. The heat flux through the sample is equated to the strain gauge's heater power output. The heater power is determined by measuring both the current provided by the current source and the voltage drop across the strain gauge. The temperature difference is measured by the thermocouples, 'zero values' of the voltage measured right before the heater is turned on are deducted from the present measurements to eliminate measurement deviations due to residual temperature gradients or voltages.

All parameters relevant to the measurement are saved in the output file – besides the effective temperature and coefficient of thermal conductivity, all resistance (and corresponding temperature) values of the involved thermocouples and temperature sensors are logged as well as heater parameters of both strain gauge and heater mats. Furthermore the set of temperature sensors that was used (Cernox™ or Pt-100 and possible error codes due to measurement problems and (in case of liquid helium cooling) the helium fill level. Lastly, time stamps corresponding to the powering on and off of the strain gauge heater are recorded; on the one hand to gauge the duration of the transient processes, on the other hand to document the measurement date; time stamps are recorded in the Unix time format. The strain gauge heater is de-powered as it is no longer needed.

When measuring and saving is completed, the program checks if the last measurement point is reached. In case of further measurements, the temperature difference between along the sample between the taps is compared to the desired value according to the sample temperature and the current table is updated accordingly. The program then advances to the next set-point in line (it increases its *range* parameter by one) and starts over by entering state `10` again.

In case the whole measurement is finished, the program enters state `0` and the shut-down process starts. All heaters are powered off (if they are still running), and the measurement process and its socket get closed.

During operation, the list of future temperature set-points and the stability criteria thereof can be changed by the `set range`, `app range` and `del range` commands. For help on the syntax of giving commands to a socket server, see section B.2.4.

The state the measurement program is currently in can be changed by the `state <xx>` command, where `<xx>` stands for the desired state. The program loop checking for the current state cycles once in about every ten seconds, this time has to be allowed for the program to react to the input. Manual changing of the program state should be an absolute exception and be done thoughtfully, unforeseen consequences can stem from haphazard changes.

An overview of the allowed program states:

`state -2:` measurement forcibly quitted
`state -1:` measurement interrupted
`state  0:` measurement end
`state 10:` set temperature set-point
`state 15:` wait for minimal allowed stability time
`state 20:` watch for temperature stability
`state 30:` start strain gauge heater
`state 40:` watch for temperature difference stability
`state 50:` calculate thermal conductivity, prepare for next cycle

B.2.3. Output Files

For each measurement, output files are generated, they are gathered in a separate directory for each measurement. The storage location can be specified in the measurement's configuration file, the recommended default location is `var/data/<sample_name>` (see figure B.1). In this directory the measurement output file, a temporary output file and separate trend line files for each measurement point are saved.

They obey the following naming convention: They all start with the string specified in the measurement's configuration file called '`FileName`'. The measurement output file gets the filename extension `.tcond`, it is therefore called `<FileName>.tcond`, a temporary file also generated ends in `.tcond.tmp`. The trend lines for each set-point are named `<FileName>_<XXX>T<Temperature>_<Y>.dat`. Therein, `<XXX>` stands for the chronologically numbered set-point in three digits, `<Temperature>` for the set-point temperature and `<Y>` for the code-letter of the monitored curve:

`A` stands for the Cernox™ sensor measuring the base temperature, `B` for the base Pt-100, `C` for the radiation shield's Cernox™, `D` for the shield's Pt-100 and `H` for the temperature difference at the thermocouples. In case of a measurement in a continuous-flow helium-cryostat, an additional curve with `<Y>` replaced by `flow` is created for the temperature measured by the cryostat's own temperature controller.

The `FileName.tcond` output file lists a status value for each measurement point. The default value is zero (and represents the absence of problems), each measurement aberrance adds its particular 'error value'. From the sum the individual problems can be determined. If this value reads not zero for a particular measurement point, the result has to taken with care. It is not necessarily wrong, but something during the measurement process did raise a warning. The status codes are:

- 0: default value, no problem
- 1: temperature stability time-out; the desired temperature stability criteria were not matched
- 2: temperature difference stability time-out; the temperature gradient along the sample did not stabilize
- 4: temperature exceeds maximum allowed value
- 8: temperature difference zero-value exceeds threshold; even without the strain-gauge heater, the sample shows a temperature gradient
- 16: maximum strain gauge heater current exceeded; a higher than allowed current was requested, instead capped at maximum value

B.2.4. Commands and Syntax

All socket servers can be given commands by command line input. It is assumed that the terminal's working directory is set to the measurement directory (`/home/thecond/measure`). The general syntax to communicate with the various devices is `python lib/writesock.py var/sockets/<socket> "<command>"`, the quotation marks around the command are compulsory. Possible choices for the `<socket>` are `Gpib`, `CurrentSrc`, `FlowCtrl`, `TempCtrl` and `ThermoCoup`. Choices for `<command>` naturally depend on the socket addressed in question. A full list of commands for every socket is available by sending the `"help"` command to the socket in question.

Bibliography

[1] N.W. Ashcroft and N.D. Mermin: *Solid State Physics*. W.B. Saunders Company (1976), ISBN 978-0030839931

[2] C. Kittel: *Introduction to Solid State Physics*. John Wiley and Sons, New York, 7$^{\text{th}}$ Edition (1996), ISBN 978-0471111818

[3] P.G. Klemens: *Theory of the Thermal Conductivity of Solids*, in *Thermal Conductivity, Vol. 1*, edited by R.B. Tye. Academic Press, London and New York (1969), ISBN 978-0127054018

[4] M. Kreuzer: *Quantum Theory*. Lecture Notes, Vienna University of Technology (2009)

[5] P.G. Klemens: *Thermal Conductivity and Lattice Vibrational Modes*, in *Solid State Physics, Vol. 7*, edited by F. Seitz and D. Turnbull. Academic Press, New York (1958), ISBN 978-0126077070

[6] P. Carruthers: *Theory of Thermal Conductivity of Solids at Low Temperatures*. Rev. mod. Phys. **33**, 92 (1961)

[7] P.G. Klemens: *The Scattering of Low-Frequency Lattice Waves by Static Imperfections*. Proc. Phys. Soc. A **68**, 1113 (1955)

[8] R. Peierls: *Zur kinetischen Theorie der Wärmeleitung in Kristallen*. Annalen der Physik **395**, 1055 (1929)

[9] J.B.J. Fourier: *Théorie analytique de la chaleur*. Chez Firmin Didot, père et fils, Paris (1822)

[10] G.F. Strouse: *Standard Platinum Resistance Thermometer Calibrations from the Ar TP to the Ag F*. Natl. Inst. Stand. Technol. Spec. Publ. 250-81 (2008)

[11] T. Yotsuya, M. Yoshitake, and J. Yamamoto: *New type cryogenic thermometer using sputtered Zr-N films*. Appl. Phys. Lett. **51**, 235 (1987)

[12] S.S. Courts, D.S. Holmes, and P.R.Swinehart: *Metal oxy-nitride resistance films and methods of making the same.* US Patent 5,367,285 (1994)

[13] *Polyimide Thermofoil™ Heaters – Data Sheet.* Minco Products, Inc., Minneapolis, URL: `http://www.minco.com/~/media/WWW/Resource%20Library/Heaters/Polyimide%20Thermofoil%20Heater%20Tech%20Spec.ashx` (visited Sept. 1 2014)

[14] *STYCAST® 2850 FT Thermally Conductive Epoxy Encapsulant – Technical Data Sheet.* Emerson & Cuming, Billerica (2001)

[15] R.L. Rosenbaum: *Some Properties of Gold-Iron Thermocouple Wire.* Review of Scientific Instruments **39**, 890 (1968)

[16] *Model 336 Temperature Controller User's Manual.* LakeShore Cryotronics Inc., Westerville, Rev. 1.3 (September 2009)

[17] K.J. Åström and R.M. Murray: *Feedback Systems: An Introduction for Scientists and Engineers.* Princeton University Press, Princeton and Oxford (2008), ISBN 978-0691135762

[18] *2400 Series SourceMeter® User's Manual.* Keithley Instruments Inc., Cleveland, Rev. K (September 2011)

[19] *Model 2182 and 2182A Nanovoltmeter User's Manual.* Keithley Instruments Inc., Cleveland, Rev. A (June 2004)

[20] Python Software Foundation, Beaverton. URL: `https://www.python.org/` (visited Sept. 1, 2014)

[21] B. Sundqvist: *Thermal diffusivity and thermal conductivity of Chromel, Alumel, and Constantan in the range 100–450 K.* J. Appl. Phys. **72**, 539 (1992)

[22] S.S. Courts and P.R. Swinehart: *Stability of Cernox™ Resistance Temperature Sensors.* Advances in Cryogenic Engineering, Vol. 45, Plenum Press, New York (2000)

[23] *Typical Cernox™ Sensitivity.* LakeShore Cryotronics Inc., Westerville, URL: `http://lakeshore.com/Documents/CX_RSDSsm.pdf` (visited Sept. 1 2014)